



U.S. Department of
Transportation
**Federal Railroad
Administration**

Identification of High-Speed Rail Ballast Flight Risk Factors and Risk Mitigation Strategies – Final Report

Office of Research
and Development
Washington, DC 20590



NOTICE

This document is disseminated under the sponsorship of the Department of Transportation in the interest of information exchange. The United States Government assumes no liability for its contents or use thereof. Any opinions, findings and conclusions, or recommendations expressed in this material do not necessarily reflect the views or policies of the United States Government, nor does mention of trade names, commercial products, or organizations imply endorsement by the United States Government. The United States Government assumes no liability for the content or use of the material contained in this document.

NOTICE

The United States Government does not endorse products or manufacturers. Trade or manufacturers' names appear herein solely because they are considered essential to the objective of this report.

REPORT DOCUMENTATION PAGE			<i>Form Approved</i> <i>OMB No. 0704-0188</i>
Public reporting burden for this collection of information is estimated to average 1 hour per response, including the time for reviewing instructions, searching existing data sources, gathering and maintaining the data needed, and completing and reviewing the collection of information. Send comments regarding this burden estimate or any other aspect of this collection of information, including suggestions for reducing this burden, to Washington Headquarters Services, Directorate for Information Operations and Reports, 1215 Jefferson Davis Highway, Suite 1204, Arlington, VA 22202-4302, and to the Office of Management and Budget, Paperwork Reduction Project (0704-0188), Washington, DC 20503.			
1. AGENCY USE ONLY (Leave blank)	2. REPORT DATE April 2015	3. REPORT TYPE AND DATES COVERED Technical Report – July 2014	
4. TITLE AND SUBTITLE Identification of High-Speed Rail Ballast Flight Risk Factors and Risk Mitigation Strategies		5. FUNDING NUMBERS	
6. AUTHOR(S) M.R. Saat, F. Bedini-Jacobini, E. Tutumluer, C.P.L. Barkan			
7. PERFORMING ORGANIZATION NAME(S) AND ADDRESS(ES) University of Illinois at Urbana-Champaign Rail Transportation and Engineering Center – RailTEC Department of Civil and Environmental Engineering 205 N. Mathews Ave Urbana, IL 61801		8. PERFORMING ORGANIZATION REPORT NUMBER DOT/FRA/BAA-2010-1	
9. SPONSORING/MONITORING AGENCY NAME(S) AND ADDRESS(ES) U.S. Department of Transportation Federal Railroad Administration Office of Railroad Policy and Development Office of Research and Development Washington, DC 20590		10. SPONSORING/MONITORING AGENCY REPORT NUMBER DOT/FRA/ORD-15/03	
11. SUPPLEMENTARY NOTES COTR:			
12a. DISTRIBUTION/AVAILABILITY STATEMENT This document is available to the public through the FRA Web site at http://www.fra.dot.gov .		12b. DISTRIBUTION CODE	
13. ABSTRACT (Maximum 200 words) The phenomenon of flying ballast is well-documented in high-speed rail operations. Displaced ballast particles from the track bed may cause damage to rolling stock as well as the track infrastructure, and wayside structures close to the right of way of the railroad. This report provides comprehensive information to help identify potential causes and hazard consequences of ballast flight, determine potential risk mitigation strategies, and define the relevance of ballast flight risks in the current and planned U.S. passenger rail system. This report presents and discusses a conceptual risk framework, which covers factors that contribute to flying ballast and the consequences of flying ballast based on the location of interest. Five relevant risk factors for flying ballast are identified: operating speed, train design, dynamic load, track maintenance, and high winds.			
14. SUBJECT TERMS Ballast flight, high-speed rail, intercity passenger rail		15. NUMBER OF PAGES 76	16. PRICE CODE
17. SECURITY CLASSIFICATION OF REPORT Unclassified	18. SECURITY CLASSIFICATION OF THIS PAGE Unclassified	19. SECURITY CLASSIFICATION OF ABSTRACT Unclassified	20. LIMITATION OF ABSTRACT

METRIC/ENGLISH CONVERSION FACTORS

ENGLISH TO METRIC

LENGTH (APPROXIMATE)

- 1 inch (in) = 2.5 centimeters (cm)
- 1 foot (ft) = 30 centimeters (cm)
- 1 yard (yd) = 0.9 meter (m)
- 1 mile (mi) = 1.6 kilometers (km)

AREA (APPROXIMATE)

- 1 square inch (sq in, in²) = 6.5 square centimeters (cm²)
- 1 square foot (sq ft, ft²) = 0.09 square meter (m²)
- 1 square yard (sq yd, yd²) = 0.8 square meter (m²)
- 1 square mile (sq mi, mi²) = 2.6 square kilometers (km²)
- 1 acre = 0.4 hectare (he) = 4,000 square meters (m²)

MASS - WEIGHT (APPROXIMATE)

- 1 ounce (oz) = 28 grams (gm)
- 1 pound (lb) = 0.45 kilogram (kg)
- 1 short ton = 2,000 pounds (lb) = 0.9 tonne (t)

VOLUME (APPROXIMATE)

- 1 teaspoon (tsp) = 5 milliliters (ml)
- 1 tablespoon (tbsp) = 15 milliliters (ml)
- 1 fluid ounce (fl oz) = 30 milliliters (ml)
- 1 cup (c) = 0.24 liter (l)
- 1 pint (pt) = 0.47 liter (l)
- 1 quart (qt) = 0.96 liter (l)
- 1 gallon (gal) = 3.8 liters (l)
- 1 cubic foot (cu ft, ft³) = 0.03 cubic meter (m³)
- 1 cubic yard (cu yd, yd³) = 0.76 cubic meter (m³)

TEMPERATURE (EXACT)

$$[(x-32)(5/9)] \square F = y \square C$$

METRIC TO ENGLISH

LENGTH (APPROXIMATE)

- 1 millimeter (mm) = 0.04 inch (in)
- 1 centimeter (cm) = 0.4 inch (in)
- 1 meter (m) = 3.3 feet (ft)
- 1 meter (m) = 1.1 yards (yd)
- 1 kilometer (km) = 0.6 mile (mi)

AREA (APPROXIMATE)

- 1 square centimeter (cm²) = 0.16 square inch (sq in, in²)
- 1 square meter (m²) = 1.2 square yards (sq yd, yd²)
- 1 square kilometer (km²) = 0.4 square mile (sq mi, mi²)
- 10,000 square meters (m²) = 1 hectare (ha) = 2.5 acres

MASS - WEIGHT (APPROXIMATE)

- 1 gram (gm) = 0.036 ounce (oz)
- 1 kilogram (kg) = 2.2 pounds (lb)
- 1 tonne (t) = 1,000 kilograms (kg) = 1.1 short tons

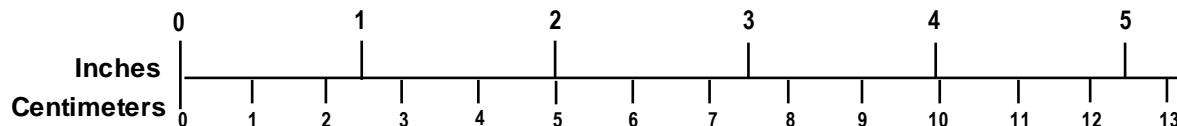
VOLUME (APPROXIMATE)

- 1 milliliter (ml) = 0.03 fluid ounce (fl oz)
- 1 liter (l) = 2.1 pints (pt)
- 1 liter (l) = 1.06 quarts (qt)
- 1 liter (l) = 0.26 gallon (gal)
- 1 cubic meter (m³) = 36 cubic feet (cu ft, ft³)
- 1 cubic meter (m³) = 1.3 cubic yards (cu yd, yd³)

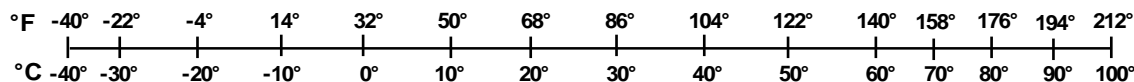
TEMPERATURE (EXACT)

$$[(9/5) y + 32] \square C = x \square F$$

QUICK INCH - CENTIMETER LENGTH CONVERSION



QUICK FAHRENHEIT - CELSIUS TEMPERATURE CONVERSION



For more exact and or other conversion factors, see NIST Miscellaneous Publication 286, Units of Weights and Measures. Price \$2.50 SD Catalog No. C13 10286

Updated 6/17/98

Table of Contents

Table of Contents	iii
List of Figures.....	iv
List of Tables	vii
Preface.....	viii
1 Introduction	1
2 Literature Review	2
2.1 Relevant Major Research Programs	2
2.2 Track Responses.....	2
2.3 Train Aerodynamics	12
2.4 Atmospheric or Weather Conditions	19
2.5 Ground Effect Conditions	21
2.6 Field Tests	22
2.7 Risk Based Models	29
2.8 Other Studies.....	34
3 Risk Framework, Factors, and Mitigation Strategies	36
3.1 Risk Framework.....	36
3.2 Risk Factors.....	37
3.2.1 Train Aerodynamics.....	37
3.2.2 Track Responses	38
3.2.3 Ground Effects	39
3.2.4 Atmospheric Conditions	40
3.2.5 Risk Prioritization	40
3.3 Consequences of Ballast Flight	42
3.4 Risk Mitigation Strategies	43
4 Ballast Flight Risk on Current and Planned U.S. Passenger Train Systems	46
4.1 Background	46
4.2 Overview of Passenger Rail Services in the United States	46
4.2.1 North East	46
4.2.2 South East	48
4.2.3 Midwest.....	49
4.2.4 West	52
4.3 Relevance of Key Ballast Flight Risk Factors.....	52
4.3.1 Operating Speed.....	52
4.3.2 Train Design.....	53
4.3.3 Dynamic Load.....	54
4.3.4 Track Maintenance Standard	55
4.3.5 High Wind.....	56
4.4 Risk Screening Tool	56
5 Summary and Conclusions	62
6 References.....	63
Abbreviations and Acronyms	67

List of Figures

Figure 2.1: Schematic model and acceleration plots at the selected points (Luo et al. 1996).....	3
Figure 2.3: Ballast box with mirror and a side view of the ballast gun (Schroeder-Bodenstein 2008).....	4
Figure 2.4: Identification of the initial particle and its velocity. The x and y-axis units are in pixels (Schroeder-Bodenstein 2008).....	5
Figure 2.5: Schematic view of SUMKA test facility with the definition of the dimensions of sections M1 to M4. Dimensions are in mm (Kaltenbach et al. 2008).....	7
Figure 2.6: Three types of trackbeds and their corresponding scale models: (a) mono-block tie with lowered ballast; (b) mono-block with no lowered ballast; (c) bi-block tie configuration (Kaltenbach et al. 2008).....	7
Figure 2.7: Number of displaced particles versus the normalized friction speed $u\tau/ut, th$ measured ahead of the test section for the three trackbeds studied (Kaltenbach et al., 2008).....	8
Figure 2.8: Model of track in a Couette flow setting (Garcia et al., 2008).....	8
Table 2.1: Data used for configuration shown in figure 2.11 (Garcia et al., 2008).....	9
Figure 2.9: Normalized velocity profiles for ballasted track (a), slab track with sand (b), and slab track with concrete (c) (Garcia et al., 2008).....	10
Figure 2.10: Velocity profiles in the ballast crib model; DB configuration (Garcia et al., 2008).....	11
Table 2.2: Numeric evaluation of the coefficient of roughness (Garcia et al. 2008).....	11
Table 2.3: Classification of the ballast shapes (Kwon and Park, 2006).....	12
Figure 2.11: Critical speeds of displaced ballast particles during the wind tunnel test (Kwon and Park, 2006).....	12
Figure 2.12: Experimental setup of the train underfloor for TGV (left) and ICE-3 (right) (Saussine and Paradot, 2008b).....	13
Table 2.4: Number of displaced particles - $U_{air} = 240$ km/h (Saussine and Paradot, 2008b).....	13
Figure 2.14: Profiles (along x) of the mean (left) and the rms (right) of the axial velocity component (Portillo et al., 2008).....	15
Figure 2.15: Schematic of the BIAC and mesh outputs used in the CFD model (Sima, 2008a).....	16
Figure 2.16: Flow field developed underneath the ICE-3 leading car (Ruter and Schroeder-Bodenstein 2008).....	17
Figure 2.17: Simulation procedure for developing flow simulations (Sima, 2008b).....	18
Figure 2.18: Plots of non-dimensional velocity relative to the ground (Sima, 2008b).....	18
Figure 2.19: PoliMI experimental setup (Diana et al. 2013).....	19
Figure 2.20: Velocity profile predictions with increasing speed (Diana et al. 2013).....	19
Table 2.5: Reported ballast projection - ballast flight incidents (Claus 2008).....	20
Figure 2.21: Train geometry and loads; measured and observed embankment Displacements at 70, 185 and 252 km/h (Madshus and Kayna 2000).....	22
Figure 2.22: Stone embedded in the nose structure (left). Damage visible on the side of the ETR 500 due to flying ballast (right) (Agretti 2012).....	23
Figure 2.23: Schematic representation of the test site at the North Entrance of the tunnel Terranuova – Le Ville (Deeg et al. 2008).....	23

Figure 2.24: Ballast pitting damage observed on UK’s HS1 railhead (left) and from a train mounted sensor (right) (Quinn et al, 2010)	24
Figure 2.25: Location of the geophones used to measure the accelerations experienced by the ties and the accelerometer used to measure the accelerations of the ballast particles (Quinn et al, 2010)	25
Figure 2.26: (a) vertical height time history of a 10 mm diameter particle; (b) vertical height and along track projection (Quinn et al 2010)	26
Figure 2.27: Lateral movement against along-track projection of a 10mm ballast particle (Quinn et al 2010)	27
Figure 2.28: Kiel probe array installed on the Seoul-Busan High-Speed Line (Kwon and Park 2006)	27
Table 2.6: Relevant parameters measured on the KTX train (Kwon and Park 2006)	28
Figure 2.29: Vertical and horizontal flow velocity profiles (Kwon and Park 2006)	28
Table 2.7: BFPF related to train speed and mass of ballast particle	29
(Kwon and Park 2006)	29
Figure 2.30: Generic Stress Strength Interface Analysis (Saussine et al., 2011)	30
Figure 2.31: PDFs of three trains (left) and of one train at two different speeds (right) (Saussine et al. 2011)	30
Table 2.8: Calculation of the risk levels based on the number of ejected particles (Saussine et al. 2011)	31
Figure 2.32: Time evolution of the phased averaged velocity (Lazaro et al. 2011)	31
Figure 2.33: Ballast projection risk as a function of normalized train speed (Lazaro et al. 2013)	32
Figure 2.34: Simulated trajectories of primary ballast particles, secondary ballast particles and cumulative number of particles displaced over time (Rueter and Schroeder-Bodenstein 2008)	33
Figure 2.35: Number of ballast particle displacements (in logarithmic scale) as a function of the train configuration (Rueter et al. 2008)	34
Figure 3.1: Ballast flight risk influence diagram	36
Figure 3.2: Example portion of an online form used to collect data through a survey at http://tinyurl.com/ballastflight	41
Table 3.1: Ballast flight risk factors and qualitative risk ratings	42
Figure 3.3: The effect of lowered ballast profile: ballast particles may be less exposed to ballast motion	44
Figure 3.4: Ballast bags placed on the Japanese Shinkansen	44
Figure 4.1: Vision for future HSR systems in the United States	46
Figure 4.2: The North East Corridor (www.amtrak.com)	47
Figure 4.3: The Keystone Corridor	48
Figure 4.4: Schematic route of the service from Miami to Orlando (All Aboard Florida, 2014)	49
Figure 4.5: The route for Chicago to St. Louis (Midwest High-Speed Rail, 2014)	50
Figure 4.6: Proposed alignment of the Chicago-Omaha corridor (FRA-Iowa ROD, 2013)	51
Figure 4.7: Route of the Chicago-Detroit corridor (Midwest High-Speed Rail, 2014)	52
Figure 4.8: The TGV and ICE 3 HS trainsets (http://4rail.net)	54

Figure 4.9: Example of HS track where no ballast particles are present on top of the sleepers. 55

Figure 4.10: The Flying Ballast Risk Evaluation Tool, Compact Version..... 57

List of Tables

Table 2.1: Data used for configuration shown in figure 2.11 (Garcia et al., 2008).....	9
Table 2.2: Numeric evaluation of the coefficient of roughness (Garcia et al., 2008).....	11
Table 2.3: Classification of the ballast shapes (Kwon and Park, 2006)	12
Table 2.4: Number of displaced particles - Uair = 240 km/h (Saussine and Paradot, 2008b)	13
Table 2.5: Reported ballast projection - ballast flight incidents (Claus, 2008)	20
Table 2.6: Relevant parameters measured on the KTX train (Kwon and Park, 2006)	28
Table 2.7: BFPF related to train speed and mass of ballast particle (Kwon and Park, 2006)	29
Table 2.8: Calculation of the risk levels based on the number of ejected particles (Saussine et al., 2011).....	31
Table 3.1: Ballast flight risk factors and qualitative risk ratings	42
Table 4.1: Qualitative severity score for operating speed ranges	58
Table 4.2: Qualitative severity score for train design (drag coefficient)	58
Table 4.3: Qualitative severity scores for the expected dynamic loads	59
Table 4.4: Qualitative severity score for track maintenance.....	60
Table 4.6: Qualitative score for countryside consequence levels	61
Table 4.7: Qualitative score for urban consequence levels.....	61
Table 4.8: Normalized weights of major risk factors	61

Preface

The phenomenon of flying ballast is well-documented in high-speed rail operations. Displaced ballast particles from the track bed may cause damage to the rolling stock, track infrastructure, and wayside structures close to the right of way of the railroad. The purpose of this report is to identify the potential causes and hazard consequences of ballast flight, review potential risk mitigation strategies, and examine relevance of ballast flight risks in the current and planned U.S. passenger rail system.

This report presents and discusses a conceptual risk framework, which covers the factors that contribute to flying ballast and their consequences based on the location of interest. The report further identifies five relevant risk factors for flying ballast: operating speed, train design, dynamic load, track maintenance, and high winds. Flying ballast is considered a risk for ballasted high-speed lines in North America. Higher speed corridors may also present a moderate level of risk of flying ballast when the appropriate conditions are met. Such conditions may include tunnel operations, snow accumulation and high-speed trains passing in opposite directions. Additional research on flying ballast should be considered when planning new high- and higher-speed rail systems.

1 Introduction

With the development of High-Speed Rail (HSR) systems around the world during the past 50 years, one of the observed phenomena that occur at the train-track interface is “ballast flight.” This phenomenon occurs when a combination of both mechanical and aerodynamic forces, generated mostly by the passage of the train, cause one or more ballast particles to overcome gravity. Flying ballast can cause damage to the railhead, train body, and adjacent structures, as well as injuries to maintenance workers and/or waiting passengers at through stations, which results in major maintenance costs and safety concerns for HSR systems with ballasted track.

The objectives of this study were to 1) investigate potential causes and hazard consequences of ballast flight, 2) identify potential risk mitigation strategies, based on international experiences, and 3) understand the relevance of ballast flight risks in the current and planned U.S. passenger rail system. The high-level mission of this study includes:

- Identifying operating and infrastructure conditions that can lead to ballast flight, and the safety implications of those conditions in HSR systems
- Enabling the development of risk assessment methodologies for HSR planners and operators that address safety and risk of ballast flight for HSR operations in the U.S.
- Enabling the development of safe and efficient HSR systems in which injuries and damage due to ballast flight can be prevented.

Chapter 2 presents a comprehensive literature review that provides insight into the current state of knowledge and identifies ballast flight risk factors. Chapter 3 presents a ballast flight conceptual risk framework and describes the identified risk factors, safety consequences, and potential risk mitigation strategies in more detail. Chapter 4 discusses the relevance of ballast flight risks in the US passenger rail system both now and in the future, and presents a semi-quantitative risk assessment model that could be used to assess the ballast flight risk relevant to specific HSR operational conditions in the U.S. Chapter 5 presents summary and conclusions.

2 Literature Review

2.1 Relevant Major Research Programs

In 2005, the French and German railways—Société Nationale des Chemins de fer Français (SNCF) and Deutsche Bahn (DB)—started the Aerodynamics in Open Air (AOA) project within a bilateral Franco-German scientific and technical research program (DEUFRAKO). AOA investigated two main issues that affect the performance and passenger comfort of trains at high speeds—the overturning effect of crosswinds at high speeds and the phenomenon of ballast projection (or ballast flight). Partners in the AOA project included, among others, train makers such as Alstom and Siemens.

Within the DEUFRAKO context, a common procedure was developed by several railroad operators to conduct measurements of flow properties underneath the carbody of a train:

- The train used for any kind of testing is to be a regular train used for normal service.
- A full classification of trains was desired in order to characterize as much as possible the likelihood of ballast movement.
- Measurement methodologies should be valid across countries that operate high-speed rail service and independent from the local environmental conditions.

In June 2009, three research projects were started under the Total Regulatory Acceptance Interoperable Network program, in response to the European Union's 2nd Call of the 7th Framework Programme to promote railway interoperability. These projects addressed the following topics: aerodynamics in the AeroTRAIN project, vehicle dynamics and track interaction in the DynoTRAIN project, and pantograph and catenary interaction in the PantoTRAIN project.

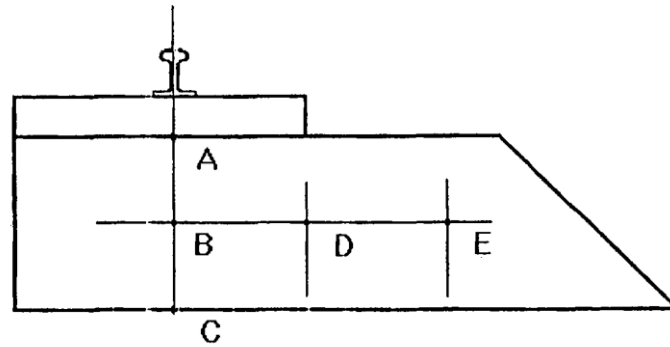
The recommendations outlined in the previously discussed AOA project were used as a starting point for a new set of laboratory and field tests conducted in France, Germany and Spain. The main purpose of the AeroTRAIN project was to establish a set of guidelines that are valid across all European countries to assess the risk of ballast flight on HSR tracks.

Reports and research papers related to ballast flight from these programs were among the literature reviewed and summarized in the following sections.

2.2 Track Responses

Luo et al. (1996) conducted a study to understand the dynamic behavior of ballast under moving trains. In order to characterize the response of the ballast particles a finite element (FE) model was developed. The rail was assumed to behave as a Timoshenko beam lying upon a discrete tie-fastening system. The ballast was modeled as a three dimensional FE model. Simulations were carried out, one that assumed a track model with no irregularities and another which assumed irregularities. Five sample points on the ballast model were taken as the measurement locations. The results for the ballast

response at the locations are shown in Figure 2.1. Among the interesting results obtained through the analysis is the behavior of ballast particles at the surface of the model (point A) that could become weightless. It was noted that with a speed of the train of 270 km/h and above, the acceleration experienced by the ballast particle at locations A and B was more than 10 m/s^2 , thus causing the “weightless condition”. A subsequent aerodynamic force would be sufficient to displace the particle.



A(0. 0.), B(0. 0.15), C(0. 0.3), D(0.15 0.15), E(0.3 0.15)

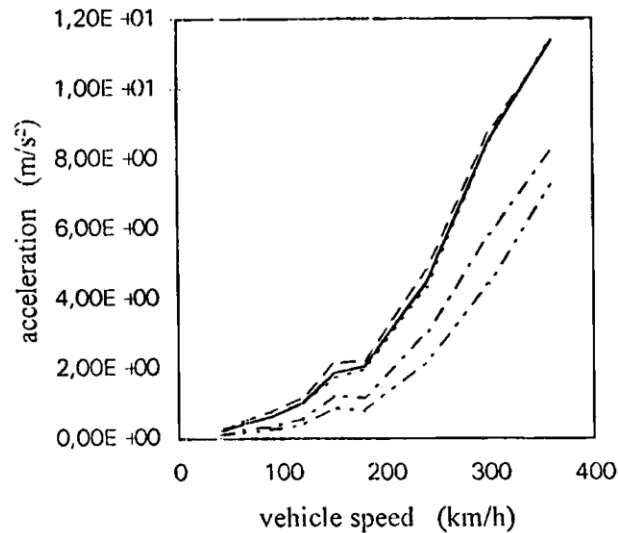


Figure 2.1: Schematic model and acceleration plots at the selected points (Luo et al. 1996)

Kaltenbach (2008a) conducted a laboratory test which measured the total work performed by an aerodynamic force that acted on a cylindrical object rolling over a sequence of small steps, which represented the typical ballast surface. A schematic representation is shown in Figure 2.2. In this case the work is related to the accumulated (stepwise) gain in potential energy of the reference body (a sphere) which should have similar size and mass as a typical ballast particle.

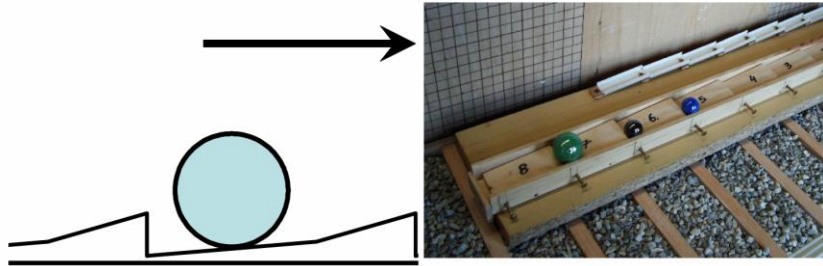


Figure 2.2: Sketch and pictures of the configuration where a reference body is climbing a sequence of small steps (Kaltenbach 2008a)

Among the main findings from Kaltenbach (2008a) is that the aerodynamic loads imposed on the trackbed are dependent on the surface conditions. A simple Coquette flow model can provide a simple estimate of the friction velocity as a function of train speed, gap width and equivalent roughness of both train underbody and track surface.

Schroeder-Bodenstein (2008) performed a study to determine the angle of restitution coefficient of a stone impacting the trackbed, and the amount of maximum height of any hit stone in the ballast crib. The set up of the experiment consisted of a “ballast gun,” which is built as a catapult. The gun shoots at an angle of 16 degrees down the horizontal plane as shown in Figure 2.3.

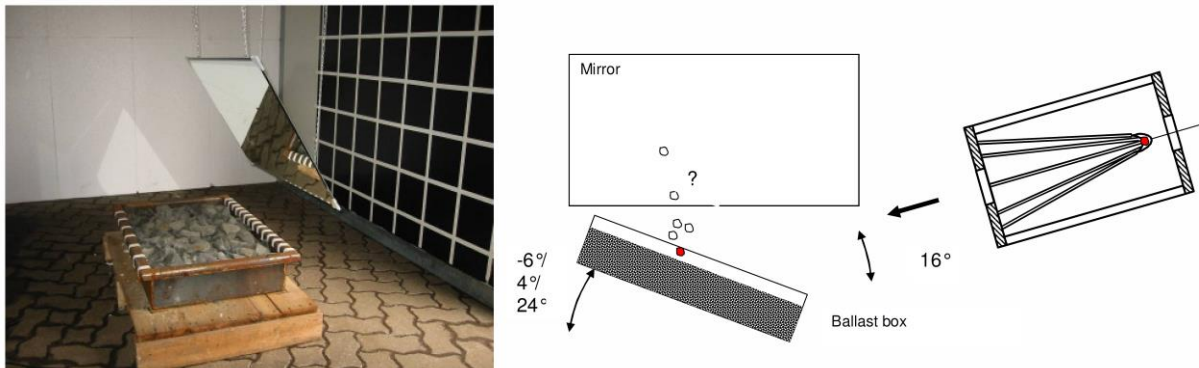


Figure 2.3: Ballast box with mirror and a side view of the ballast gun (Schroeder-Bodenstein 2008)

Figure 2.4 shows the path produced by several superimposed frames of a stone “fired” by the ballast gun. From the preliminary results obtained, a degree of “destructiveness” was measured. Probability density functions (PDFs) developed in the report show that there was a high likelihood that the ballast particle hitting the crib at 150 km/h would disintegrate, while a lower likelihood of destruction was observed at low impact speeds.

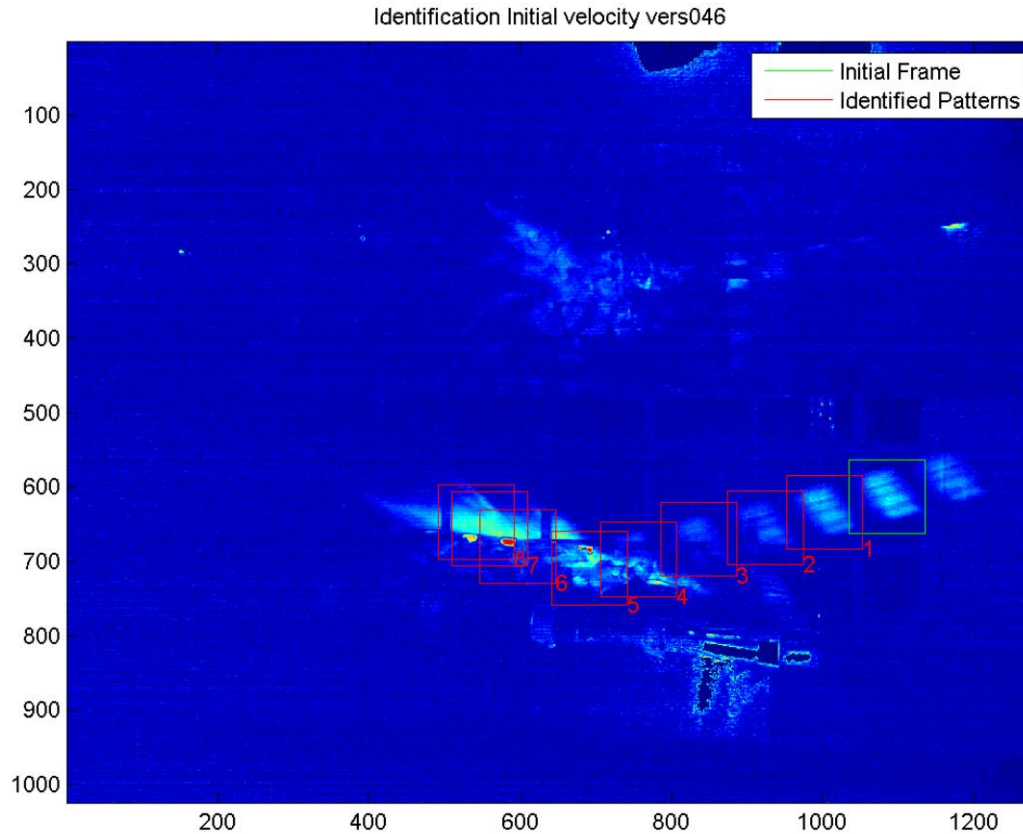


Figure 2.4: Identification of the initial particle and its velocity. The x and y-axis units are in pixels (Schroeder-Bodenstein 2008)

Additional testing with the ballast gun revealed that the kinetic energy released appears to present a linear relationship with respect to the number of stones ejected. An impact angle of 20 degrees from the horizontal plane produces an average kinetic energy of about 100J and two stones were ejected. At a kinetic energy of 500J, seven stones were ejected. The angle of impact appeared to be an important factor in ballast projection. If the angle of impact is 40 degrees, there is a likelihood of 90 percent that the stone will be destroyed at impact with the crib (Schroeder-Bodenstein, 2008).

Saussine and Paradot (2008a) performed a similar study to that of Schroeder-Bodenstein (2008). They analyzed the collision of ballast particles using numerical simulations. After conducting 3,564 numerical simulations, a relationship representing the number of ejected stones as a function of their kinetic energy was established:

$$N_{ej}(\alpha_i, E_{ci}) = F(\alpha_i)E_{ci} + N_{cst}(\alpha_i)$$

where:

- N_{ej} is the number of stones ejected from the ballast bed;
- α_i represents the angle of impact of the projected stone onto the ballast;
- E_{ci} is the kinetic energy of the impacting stone;

- N_{cst} is the coefficient of restitution function defined as

$$\begin{cases} N_{cst}(\alpha_i) = -0.0007\alpha_i^2 + 0.0992\alpha_i - 2.6742 & \alpha_i \in [0,40] \\ N_{cst}(\alpha_i) = -0.0014\alpha_i^2 + 0.0573\alpha_i + 0.0712 & \alpha_i \in [40,90] \end{cases}$$

With a coefficient of restitution of 0.99 and 0.95 respectively;

- $F(\alpha_i)$ is a linear relationship of the angle of impact defined as follows:

$$\begin{cases} F(\alpha_i) = 0.0007\alpha_i + 0.0022 & \alpha_i \in [0,30] \\ F(\alpha_i) = -0.0001\alpha_i + 0.0249 & \alpha_i \in [30,90] \end{cases}$$

Since the velocity of the particle can be characterized by the orthogonal components, a global coefficient of restitution, e , was suggested under the three spatial relationships and tested against the results obtained in Schroeder-Bodenstein (2008). From physics, the coefficient of restitution can be defined as the ratio of the velocity of the body before impact, V_i , and the velocity of the same body after impact V_e :

$$e = \frac{V_e}{V_i}$$

Based on the simulations conducted by Saussine and Paradot (2008a), the best fit for the data obtained was presented as follows:

$$e(\alpha_i) = 0.0001\alpha_i^2 - 0.211\alpha_i + 0.9964$$

It was noted that the coefficient of restitution decreased as the angle of impact increased, which agrees with the tendency of the ballast stones behave somewhat elastically.

Finally, three PDFs, used to estimate the likelihood of the velocity of a stone after impact, were tested. The three PDFs follow a normal curve. However, when the output of the PDFs were compared to the experimental data obtained by Schroeder-Bodenstein (2008), it was determined that there was no agreement between the two data sets. Among the conclusions stated by Saussine and Paradot (2008a) was that additional research into PDFs is needed to establish better correlation with experimental results.

The effect of the vibration of the ties was analyzed in Saussine and Paradot (2008b). According to their research, an input amplitude of 6 mm and an input frequency of 3 Hz led to a 10 percent increase in the number of flying particles.

Kaltenbach et al. (2008) conducted an experimental investigation of ballast motion using a 1:10 scale track model in a SUMKA test facility (Figure 2.5).

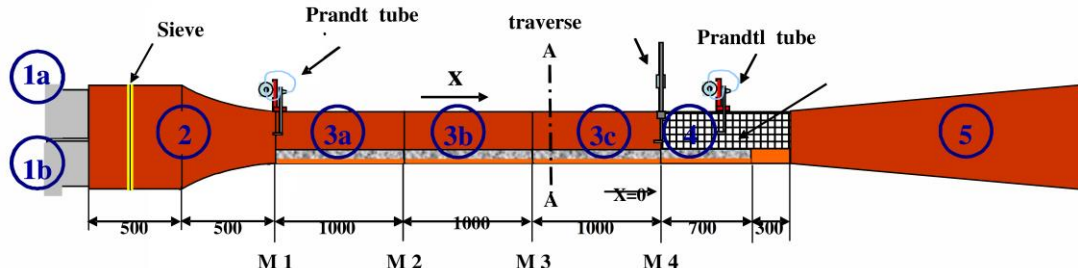


Figure 2.5: Schematic view of SUMKA test facility with the definition of the dimensions of sections M1 to M4. Dimensions are in mm (Kaltenbach et al. 2008)

Figure 2.6 shows three different type of trackbed models placed in the 30 mm wide and 70 mm long test section. The 1:10 scale models represent roughly three trackbed conditions: mono-block sleepers with the ballast level lowered by 40 mm below top of sleepers (a), with the ballast level flush with the sleeper surface (b), and bi-block sleepers (c). For a given flow speed over the bed, the numbers of particles displaced during $T_{exp} = 6 \text{ min}$ of steady blowing were counted. Prior to each experiment, the bed was placed on a mechanical shaker for about 30 s in order to simulate the process of “solidification” due to the dynamic excitation by passing trains. In addition, the perched objects which are not representative for the bed status were blown off for 30 s. Each experiment was repeated three times.



Figure 2.6: Three types of trackbeds and their corresponding scale models: (a) mono-block tie with lowered ballast; (b) mono-block with no lowered ballast; (c) bi-block tie configuration (Kaltenbach et al. 2008)

The results indicated that the track with the bi-block tie was the most prone to flying ballast (Figure 2.7).

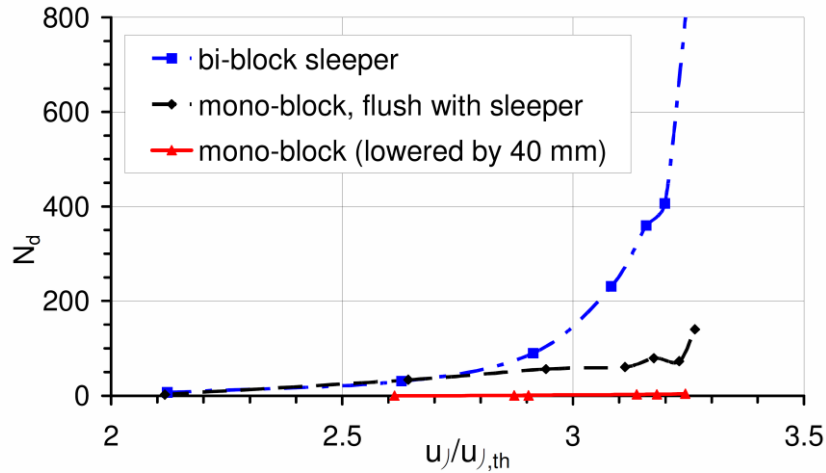


Figure 2.7: Number of displaced particles versus the normalized friction speed $u_{\tau}/u_{\tau,th}$ measured ahead of the test section for the three trackbeds studied (Kaltenbach et al., 2008)

The data was generated by measuring the air speed immediately before the test section. The air speed was then normalized with the air threshold speed $u_{\tau,th}$ value determined by the following relationship:

$$u_{\tau,th} = A \times \sqrt{\frac{\rho_s - \rho_A}{\rho_A} \times d_p \times g} \quad A = 0.1$$

Where $u_{\tau,th}$ is the threshold friction velocity, and ρ_A and ρ_s are the densities of the air and gravel respectively. The main conclusion drawn from this study is that a lower ballast profile with respect to the top of the tie greatly reduces ballast particle motion. The type of tie used was also observed to have a significant influence.

Another trackbed modeling experiment was also performed by the Universidad Politécnica de Madrid (UPM) (Garcia et al., 2008). A simplified track model was implemented (Figure 2.8) and the flow was assumed to be a Couette flow. The ballast between the tracks was modeled with an equivalent roughness coefficient k_s and other parameters are shown in Table 2.1.

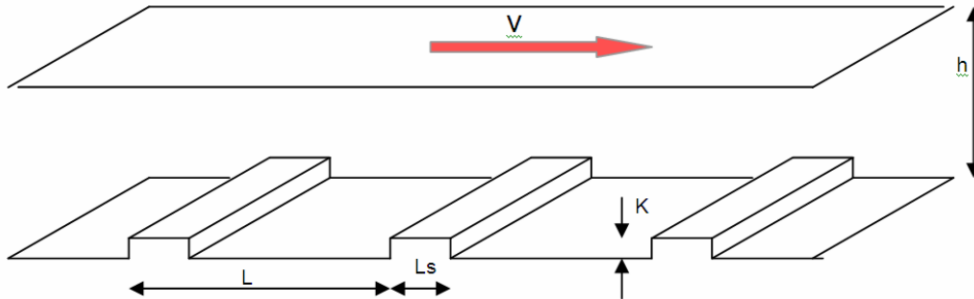


Figure 2.8: Model of track in a Couette flow setting (Garcia et al., 2008)

Table 2.1: Data used for configuration shown in figure 2.11 (Garcia et al., 2008)

Set of parameters	h (m)	L (m)	L_s (m)	K (m)	V (km/h)
Deutsche Bahn	0.40 0.38	0.62	0.127	0.04 0.02	275
SNCF	0.40 0.38	0.6	0.29	0.04 0.02	275

A typical solution is shown in Figure 2.9 where the following equations describing a fully rough wall was used:

$$u^+ = 2.5 \ln z^+ + 8.5 - 2.5 \ln \frac{k_s u^*}{v}$$

where:

- u^* is the friction velocity obtained by numerical means;
- $u^+ = \frac{u}{u^*}$, where u is the flow velocity;
- $z^+ = \frac{z u^*}{v}$, where z is the distance to the wall;
- k_s is the equivalent roughness coefficient;
- $v = 0.14 \times 10^{-4} \text{ m}^2/\text{s}$ is the kinematic viscosity of air.

The equation is valid only in the neighborhood of the lower wall (the track surface). To describe the flow behavior u of this region, the authors proposed the following closed form relationship to describe the velocity profile of the flow:

$$u = 2.5 u^* \left(\ln \left(\frac{\sin \frac{\pi z}{2h}}{\frac{\pi z_{01}}{2h}} \right) - \ln \left(\cos \frac{\pi z}{2h} \right) \right)$$

where:

$$u^* = \frac{V}{2.5 \left(\ln \frac{2h}{\pi z_{01}} + \ln \frac{2h}{\pi z_{02}} \right)}$$

and the shear stress ρu^{*2} is uniform across the gap between the ties. The velocity profile is shown in Figure 2.10.

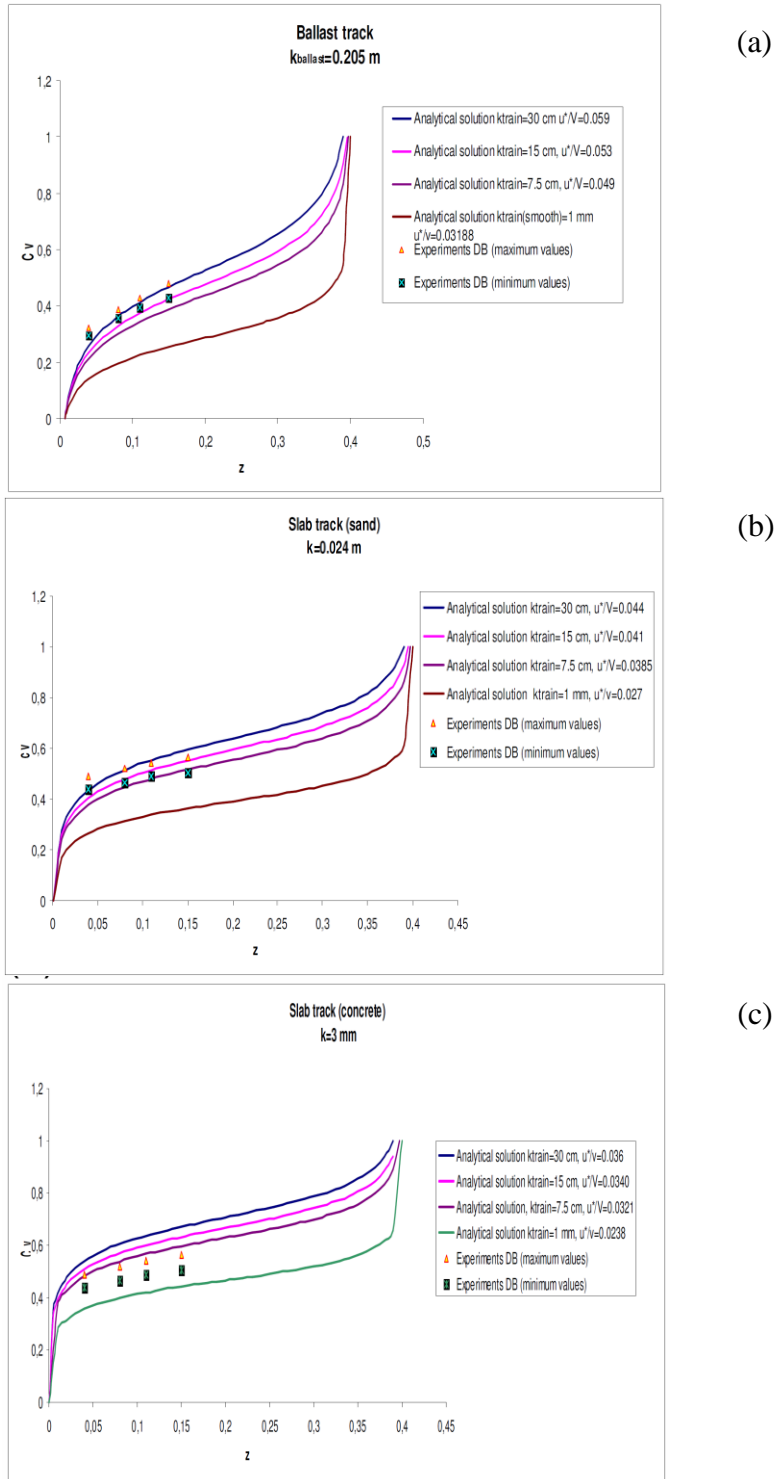


Figure 2.9: Normalized velocity profiles for ballasted track (a), slab track with sand (b), and slab track with concrete (c) (Garcia et al., 2008)

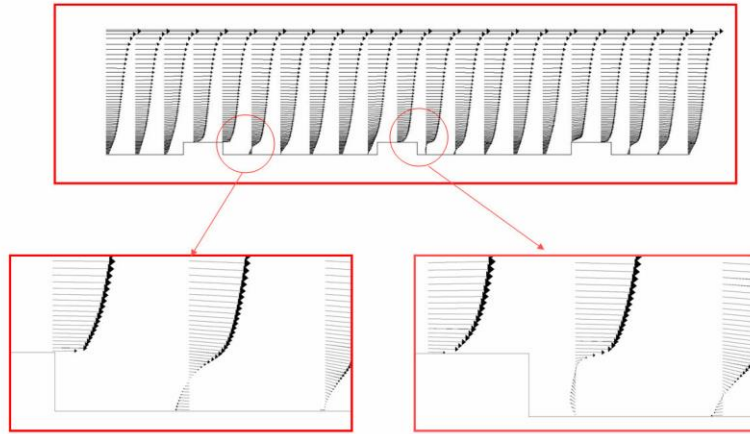


Figure 2.10: Velocity profiles in the ballast crib model; DB configuration (Garcia et al., 2008)

In Figure 2.10, the velocity profile is close to the ballast crib in between the modeled ties. Although the proposed model is two-dimensional, it reproduces a vortex effect which could affect the lift of ballast particles in the crib. The equivalent coefficient of roughness can be then computed and compared to data obtained by SNCF and DB (see Table 2.2). It can be seen that the calculated parameter u^* has similar values.

Table 2.2: Numeric evaluation of the coefficient of roughness (Garcia et al. 2008)

	K (m)	B	u^* (m/s)	u^* (m/s) eq. (3.2.4)	k_s (m)	z_0 (m)
DB track	0.04	-16.19	1.900	1.851	0.15	5e-3
	0.02	-11.85	1.726	1.701	2.89e-2	9.63e-4
SNCF track	0.04	-17.05	1.953	1.882	0.205	6.83e-3
	0.02	-14.28	1.824	1.784	7.258e-2	2.42e-3

Kwon and Park (2006) conducted wind tunnel experiments that analyzed ballast flying as caused by strong winds from the passage of high-speed trains. About 1,000 ballast particles were collected from the high-speed line between Seoul and Busan, and 330 of them were classified according to their mass and shape. The particles were then placed in a wind tunnel, where the researchers analyzed the relationship between their mass and shape properties and the aerodynamic effect. During the tests, the movement of the ballast particles was observed by increasing the wind speed. The velocities at which ballast particles started to move were recorded as critical speeds. Table 2.3 describes how the ballast particles were classified. Figure 2.11 presents the critical speed at which ballast particles began to move as a function of their ballast mass.

Table 2.3: Classification of the ballast shapes (Kwon and Park, 2006)

Type	Definition	Aerodynamic Property	Illustration
A	Flat	Very variable as the direction of wind	
B	Half-spherical	Variable as the direction of wind	
C	Spherical	Slightly variable as the direction of wind	

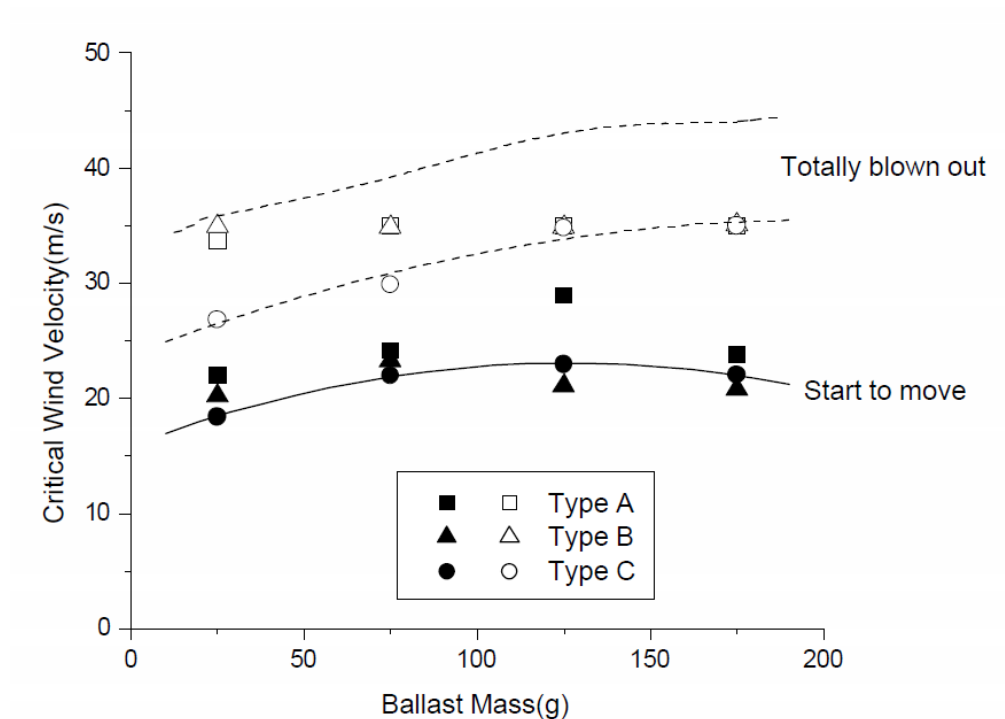


Figure 2.11: Critical speeds of displaced ballast particles during the wind tunnel test (Kwon and Park, 2006)

2.3 Train Aerodynamics

Saussine and Paradot (2008b) performed a full scale laboratory test in Nantes (France) to reproduce a ballasted track, the geometry of the train underfloor, the intercar gap of a TGV and ICE-3 trainset (Figure 2.12), and the gust effect. To simulate the gust effect, a special shutter system was installed on the track model.

The statistical distribution of ballast particles displaced by the wind gusts with an imposed air speed of 240 km/h are shown in Table 2.4. The results show that there was no flying ballast at air speeds below 180 km/h, while at a reference air speed of 240 km/h, 15 particles became airborne. The intercar gap was also simulated, and it was noted that the presence of an intercar gap reduced the number of flying ballast particles as it provides an “escape door” to the highly turbulent airflow underneath the train.



Figure 2.12: Experimental setup of the train underfloor for TGV (left) and ICE-3 (right) (Saussine and Paradot, 2008b)

Table 2.4: Number of displaced particles - $U_{air} = 240$ km/h (Saussine and Paradot, 2008b)

Displacement interval (cm)	Particles displaced	Percentage of total
0	1	4
20	4	17
40	4	17
500	15	63
Total	24	100

A great amount of effort has been devoted to implementing numerical solutions capable of characterizing the turbulence that is formed underneath the train, including the Reynolds Average Navier Stokes (RANS), Large Eddy Simulation (LES), and Detached Eddy Simulation (DES) solutions. A brief description of three solutions is provided below (Kundu and Cohen, 2008).

The RANS equations are time-averaged equations of motion of fluid flow. They are based on the so-called Reynolds decomposition, by which the steady component of a flow is separated from its turbulent component. The Reynolds decomposition may be represented by the following relationship:

$$u(x, y, z, t) = \overline{u(x, y, z)} + u'(x, y, z, t)$$

u , represents the flow, \bar{u} is the steady component of the flow, and u' is the perturbing component. The interesting property of this decomposition is that the time mean of u' is zero.

The Navier-Stokes (NS) equations represent the governing laws of motion in an incompressible Newtonian fluid. The original equations represent an instantaneous state of the flow. It is beyond the scope of this report to go into the details of the equations. It is sufficient to note that the Reynolds decomposition can use the NS equations to obtain a new set of equations that satisfy the purpose of capturing macroscopic behavior of fluids and their turbulences. The new set of equations can then be implemented in computer simulations that are able to produce good quality numeric solutions.

Large Eddy Simulation (LES) is a computational implementation of the NS equations. The implementation is done through a process called low-low pass filtering, which is used to remove small scales of the solution to the NS equations. LES resolves large scales of the flow field solution allowing better fidelity than alternative approaches such as RANS. It also models the smallest scales of the solution. The computational effort is however extremely high, especially when complex models such as trains on track are simulated.

Detached Eddy Simulation (DES) is a modification of a RANS model in which the model switches to a subgrid scale formulation in regions fine enough for LES calculations. Regions where the turbulent length scale is less than the maximum grid dimension and are near solid boundaries are assigned the RANS mode of solution. As the turbulent length scale exceeds the grid dimension, the regions are solved using the LES model. Therefore the grid resolution is not as demanding as pure LES, thereby considerably reducing the computational cost.

The simplest way to represent a flow behavior between the train and the track is through the Couette flow model. It assumes that the flow is confined by two infinite plates, one of which is not moving while the other one has a velocity v . The resulting flow is laminar and in a steady state. The complications arise when parts underneath the train and the track surface have to be modeled, since now turbulences are introduced.

Portillo et al. (2008) developed a simple simulation model that reproduces the aerodynamic behavior of the train when the bogies (or trucks) are included. The model is called Bogies in A Channel (BIAC). Figure 2.13 illustrates the schematic outline of the physical model. The experiment was tailored around existing 1:7 scale wooden models of

two typical ICE 3 bogies. The generic underfloor geometry includes typical flow features of the underfloor region of a train which challenge computational fluid dynamics (CFD).

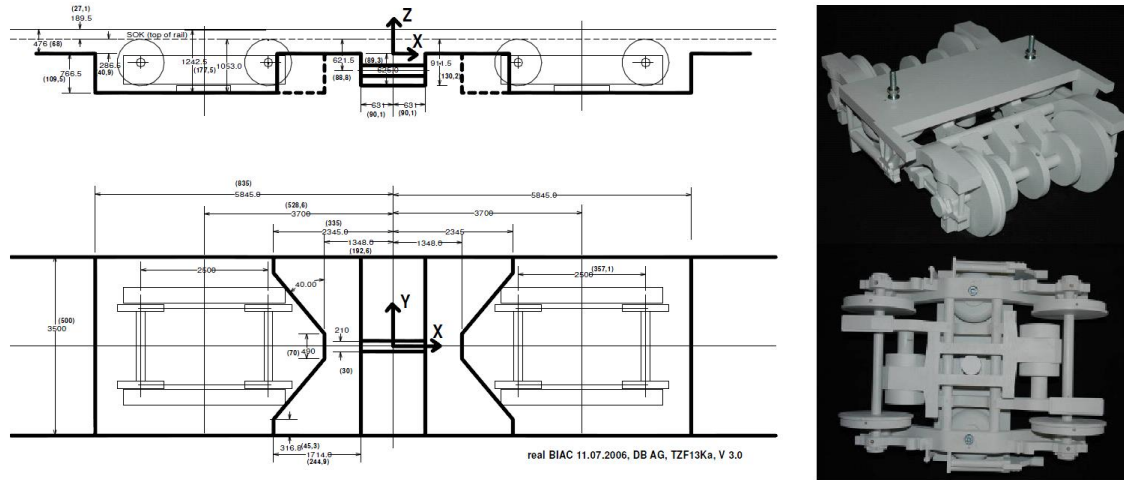


Figure 2.13: Schematic underfloor geometry of the BIAc; a 3D representation of a bogie (Portillo et al., 2008)

Figure 2.14 shows the mean values and rms. of the axial velocity component at several lateral positions close to the flat wall of the rig ($z/h = 0.91$) which represents the trackbed. Both the horizontal and vertical axis were normalized to the height of the bogie with respect to the trackbed and the reference velocity of 25.5 m/s respectively.

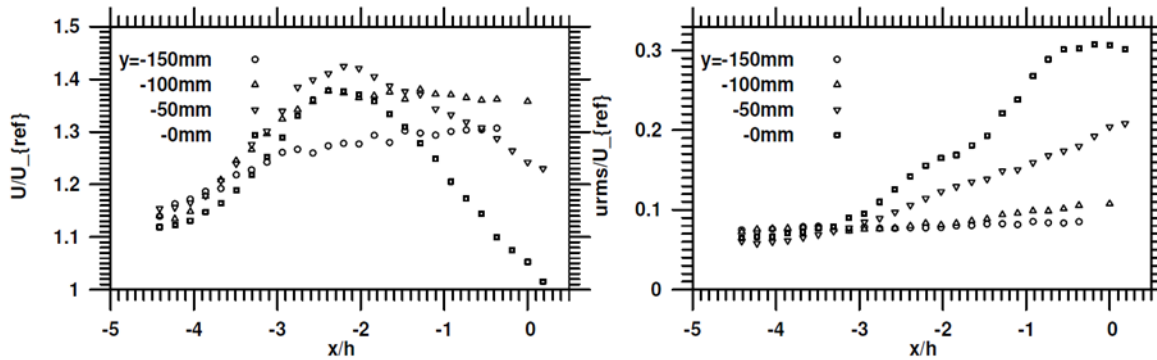


Figure 2.14: Profiles (along x) of the mean (left) and the rms (right) of the axial velocity component (Portillo et al., 2008)

Based on the considerations outlined in the previous paragraphs, there is a need to determine the best-practice procedure for producing the most accurate simulation of an underfloor flow using CFD. The key steps can be summarized as follows:

- Simplification of the geometrical surface data
- Defining a computational mesh
- Choice of turbulence model and convective discretization
- Domain setup and simplifications

The above suggested procedures have been first implemented in the study of the flow of a bogie in a channel in Portillo et al. (2008).

Sima (2008a) proposed the following implementation of mesh design of train bogies for the purposes of ballast projection phenomena. The geometries should resemble a generic underfloor with two bogies and an intercar gap at a 1:7 scale representation. For the computational approaches, the suggestion was to use a steady state RANS or Transient DES approaches. Figure 2.15 illustrates the computational domain and motor bogie reference mesh using the BIAC approach.

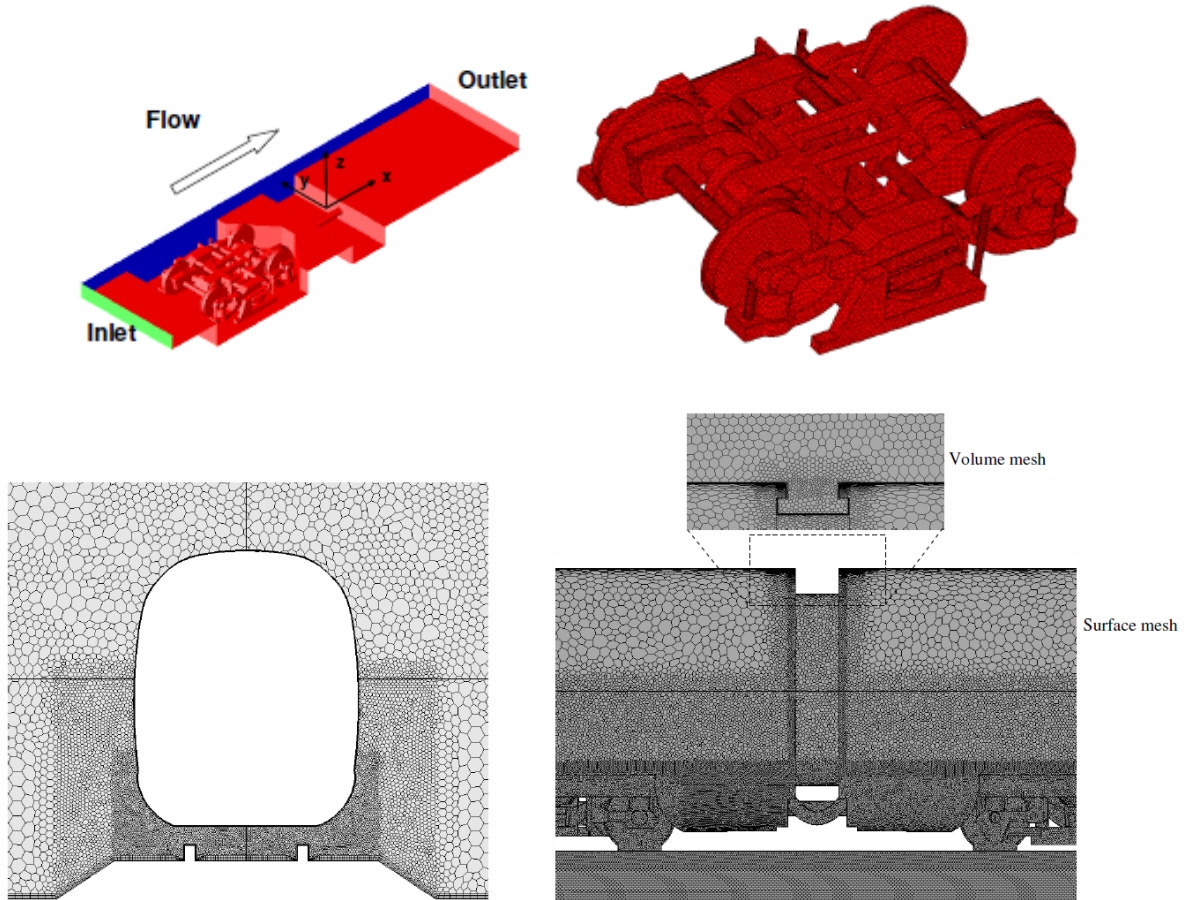


Figure 2.15: Schematic of the BIAC and mesh outputs used in the CFD model (Sima, 2008a)

The models presented above are used to validate turbulence models for a generic underfloor geometry. Turbulence models developed using RANS were too low in accuracy compared with those developed using a DES and LES approach. Also, shear stress on the track is considered an important parameter when studying the motion of ballast particles due to either projection of foreign objects or liftoff due to aerodynamic forces. Shear stresses may also vary between train models.

Ruter and Schroeder-Bodenstein (2008) performed a full-scale measurement of the front of the ICE 3. The implementation adopted a RANS model and BIAC as the reference model of the bogie. The first half of the leading ICE 3 car was studied in detail in order to set the framework for understanding the flow buildup in the subsequent sections of the full train. The relevant results of this study are shown in Figure 2.16. The flow field around the lower portion of the train was used as an input field for modelling the flow of the subsequent cars. Figure 2.16 shows the normalized output velocities. The reference velocity is the speed V of the train. Figure 2.16 also shows the wake effect created and used as an input to study the air motion underneath the trailing cars.

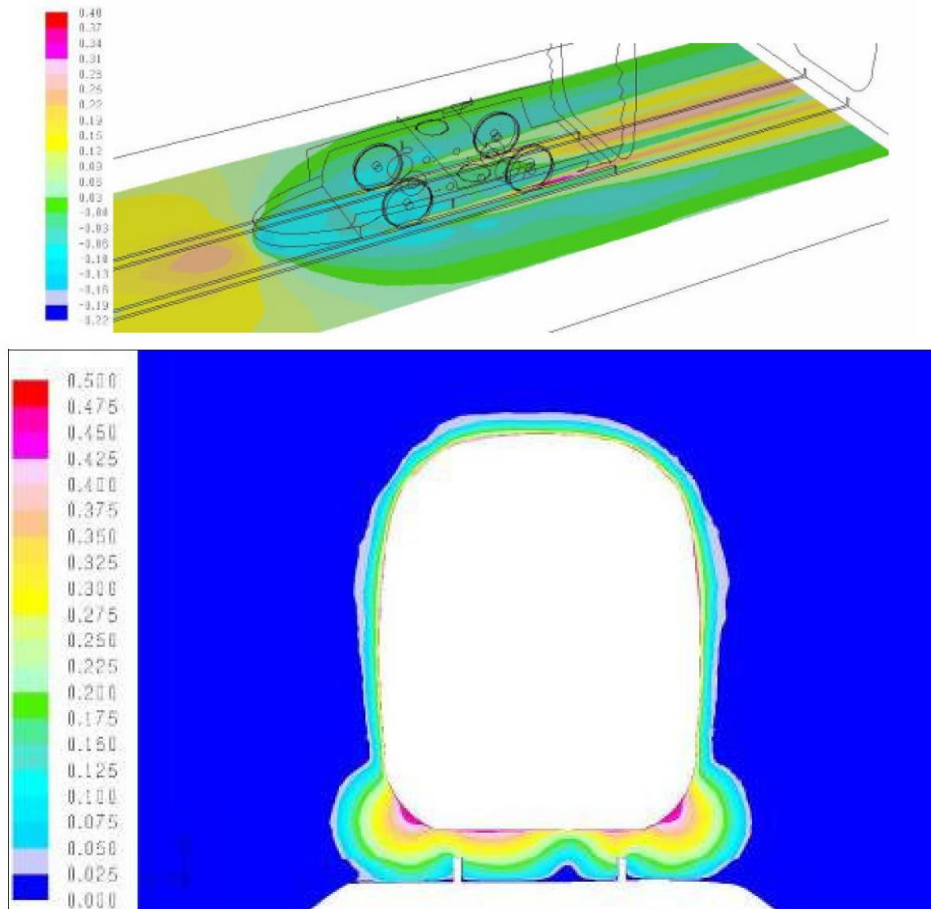


Figure 2.16: Flow field developed underneath the ICE-3 leading car (Ruter and Schroeder-Bodenstein 2008)

A detailed study of the underfloor flow was conducted by Sima (2008b). The model comprised of two half mid-cars connected by the typical train gap. The approach used a three step simulation. A simulation using DES was not implemented due to budget constraints and time available for the study. The RANS implementation however produced results with a good degree of accuracy. The input flows were implemented using the “marching technique” where the wake effects of the leading section of the train

was used as inputs into the next section. A schematic representation of the “marching technique” is shown in Figure 2.17.

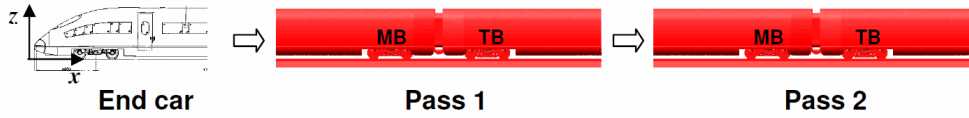


Figure 2.17: Simulation procedure for developing flow simulations (Sima, 2008b)

The BIAC model was again used to simulate the flow between the bogies of the two adjacent cars. Figure 2.18 shows the velocity profile relative to the ground as an output of the motion of the train. The locations of interest are at the front of the bogie and at 1.5 meters from the front. The asymmetry shown was likely due to the level of detail of the modelling of the bogie.

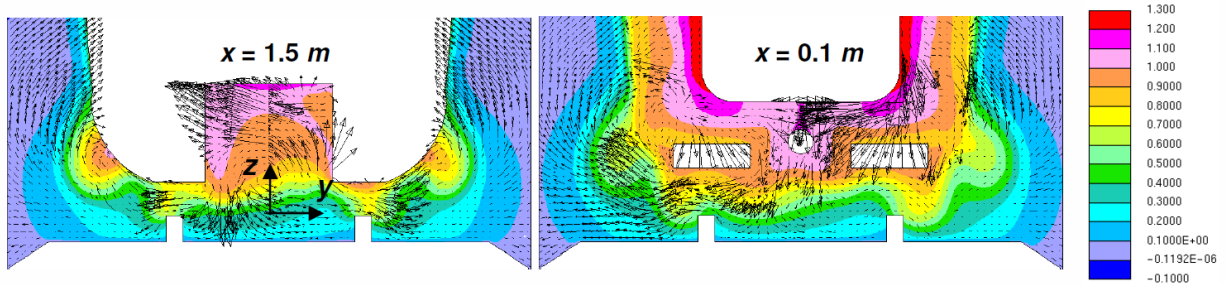


Figure 2.18: Plots of non-dimensional velocity relative to the ground (Sima, 2008b)

Further applications of this modelling have been implemented and conducted at the Politecnico di Milano (PoliMI) in Italy (Rocchi et al., 2008). The high-speed train ETR 500 was modeled using the same “marching technique”. The experimental results agreed in general with those in Sima (2008b). In both cases, the shear stress experienced by the ballast particles appeared to be a contributing factor.

Diana (2013) further developed CFD modelling by applying the technique to one single train as opposed to portions of the train. Currently, there is an ongoing feasibility study to increase the commercial speed of the Italian high-speed lines from 300 to 360 km/h. A new field test setup has been implemented with a new measuring device, a pressure cube (Figure 2.19). This device can capture pressures in 3D as opposed to previous test campaigns, in which static Pitot tubes were used to capture unidimensional data.

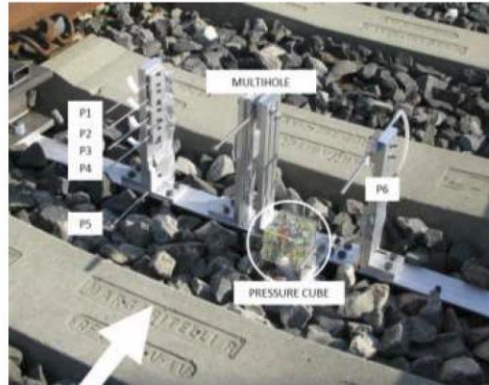


Figure 2.19: PoliMI experimental setup (Diana et al. 2013)

The simulation results using a 20 million CFD mesh are shown in Figure 2.20.

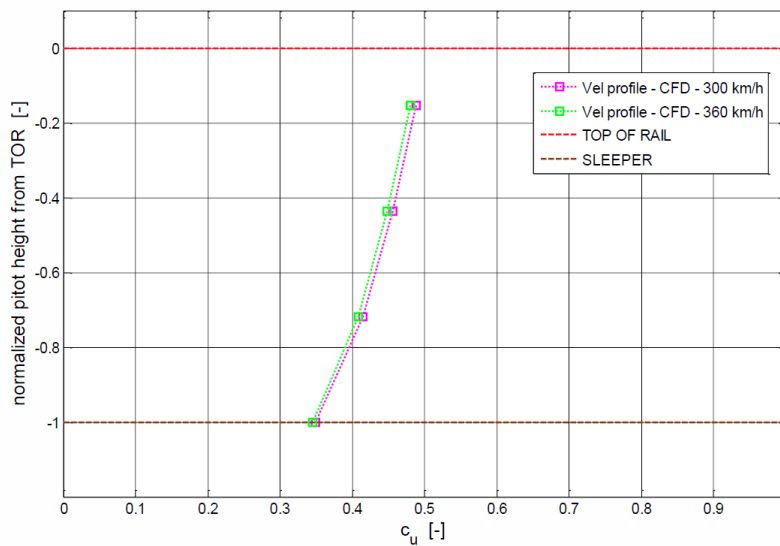


Figure 2.20: Velocity profile predictions with increasing speed (Diana et al. 2013)

2.4 Atmospheric or Weather Conditions

Ballast projection instances have been reportedly caused by meteorological conditions such as ice formation or snow. As the operating speed of the trains increased to 300 km/h and above, damage to trains and infrastructure was noted to occur at standard meteorological conditions as well. Table 2.5 is a summary of known occurrences of ballast projection. Claus (2008) further reports that SNCF did not record any ballast flight incident over the past 20 years. No ballast flight was observed or recorded during the 2007 test runs performed by the TGV V-150 when it successfully achieved the world speed record.

Table 2.5: Reported ballast projection - ballast flight incidents (Claus 2008)

Date	Train type	Location	Speed (km/h)	Speed (mph)	Track type	Weather conditions	Remarks
2001	ICE3	Fulda - Gottingen, Germany	230	143	Mono- block ties, lowered ballast	Winter conditions, snow	
2003	KTX	South Korea	300	186	Mono- block ties	No snow	See Kwon and Park (2006) for details
2003	ICE3	Lille - Calais, France	320	199	Bi-block ties	Winter conditions, snow	
2003	ICE3	Belgium	300	186	Mono- block ties, ballast not lowered	No snow	Speeds up to 275 km/h did not cause problems in double traction
2004	ICE3	France	320	199	Bi-block ties		During homologation test runs
2004	ICE3	Mannheim - Stuttgart, Germany	250	155	Mono- block ties, lowered ballast	Winter conditions, snow	Foreign parts in the track have been found
2004	ETR500	Rome - Naples, Italy	300	186	Mono- block ties, ballast not lowered	No snow	New track with ballast above ties
2006	ICE-T	Hamburg - Berlin, Germany	230	143	Mono- block ties, lowered ballast	Winter conditions, snow	

2.5 Ground Effect Conditions

Ground effect motion or ground vibration induced by the passage of trains does not by itself initiate the motion of ballast particles. However, it can be a contributing factor when combined with aerodynamic effects. One of the aspects that emerged during the past two decades is the so-called “critical speed” of the train. As noted in Krylov (1995), the train is travelling at a critical speed when its speed matches the speed of the Rayleigh waves. In his study, Krylov analyzed the effects of trains at different speeds when travelling on different types of soil. For example a soft sandy soil would have a Rayleigh wave speed between 90 and 130 m/s. Significant ground vibrations could be expected for trains travelling at 300 km/h (83 m/s). The ground response would resonate with the input vibration from the train. The author also simulated the ground motion effects caused by a moving train. Experimental observations performed by Krylov (2000) of a Swedish X2000 train that generated a ground boom at 180 km/h confirmed the critical speed theory.

Madshus and Kayna (2000) showed that large dynamic amplifications appear in the dynamic response of the rail, embankment, and/or ground system as the train speed approaches a critical value that corresponds roughly to the Rayleigh waves. A series of tests was conducted on a site consisting of weathered clay crust over a very soft organic clay over soft marine clays. The embankment was about 1.4 m from the top of the rail. A total of 20 test runs were performed at several different speeds ranging from 70 to 252 km/h. It was observed that the displacement experience by the embankment increased drastically as the train speed increased above a certain value. Figure 2.21 displays a summary of the measured and simulated displacements of the embankment and it is evident that magnitude of the displacements increases as the speed of the train increases. When the train reaches or exceeds the critical speed (in this case 235 km/h), the input waves generated by the passage of the train are either in resonance with the Rayleigh ground waves or out of phase.

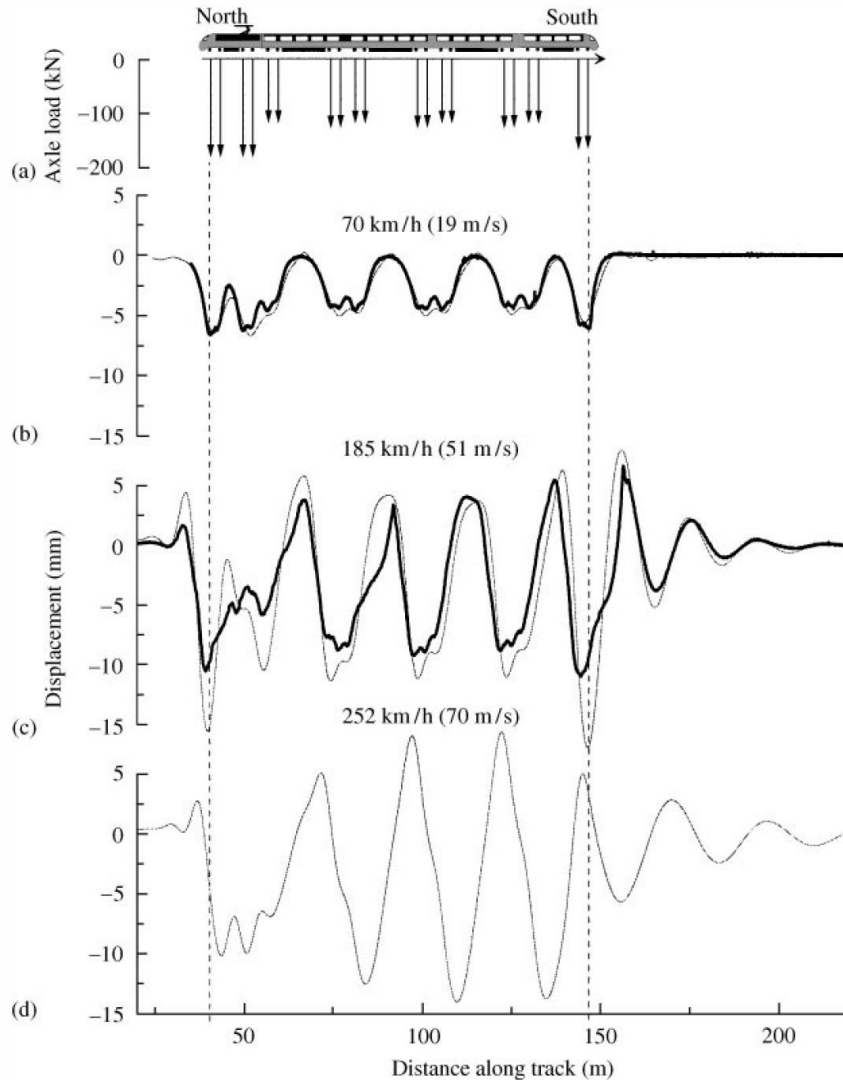


Figure 2.21: Train geometry and loads; measured and observed embankment Displacements at 70, 185 and 252 km/h (Madshus and Kayna 2000)

Within the context of flying ballast, the subgrade's dynamic behavior will most likely influence the dynamic behavior of the ballast particles. These observations can be further supported by the dynamic analysis presented earlier in this report (Luo et al. 1996).

2.6 Field Tests

The following paragraph summarizes an interview with electrical engineer Marco Agretti (from the Italian civil engineering firm Sirti). In 2004, the Italian State Railways (FS) was certifying the newly constructed high-speed line between Rome and Naples for operations at 300 km/h. One of the components that underwent the certification process was the European Rail Traffic Management System/European Train Control System level 2 signal and control system. The tests were conducted using a standard ETR 500 trainset in its typical composition of 11 cars and two locomotives. Tests were carried out at speed

increments starting from 80km/h. At 270 km/h, damage occurred to the lateral carbody and the bogies. Sudden impacts to the train were felt at approximately the fourth or fifth car of the trainset. Stones were found embedded in the nose of the locomotive. However, no damage was reported at speeds below 260 km/h. Figure 2.22 shows the damage caused to the train by a particle. The meteorological conditions at the time of the test runs were normal, thus the damage was caused by ballast particles being picked up as a result of the turbulent flow combined with the normal track response to moving loads. The railroad infrastructure manager, Rete Ferroviaria Italiana (RFI), decided to adopt a measure that was already in place on the French high-speed lines—lowering the ballast profile. The flying ballast ceased after the profile was lowered.



Figure 2.22: Stone embedded in the nose structure (left). Damage visible on the side of the ETR 500 due to flying ballast (right) (Agretti 2012)

In spring 2006, Deeg et al. (2008) conducted a field test in Italy to assess the relevance of the shear stress parameter. The location for the test was the north entrance of the Terranuova-Le Ville tunnel, along the “Direttissima” Rome-Florence high-speed line. At that location, the maximum allowed speed ranged between 140 and 250 km/h depending upon the type of train. The test section, as shown in Figure 2.23, included a portion of ballasted track and a portion of slab track.

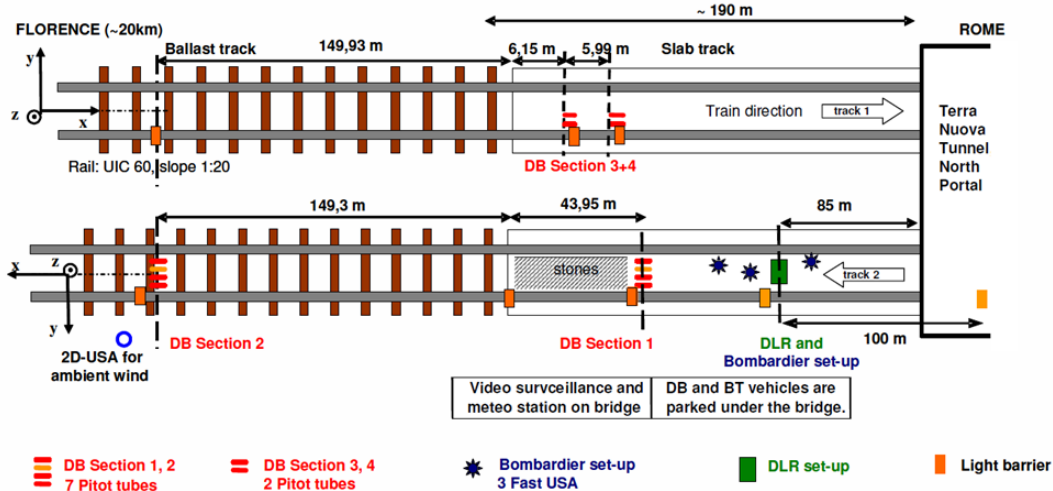


Figure 2.23: Schematic representation of the test site at the North Entrance of the tunnel Terranuova – Le Ville (Deeg et al. 2008)

To conduct the measurements, a series of ultrasonic two-component anemometers were used, as well as the vertical and horizontal rakes of Pitot and Prandtl tubes. Among the main conclusions drawn from the test was that a change in roughness of the trackbed modifies the mean axial flow in accordance with the common knowledge of flow along rough plates. Pitot rake measurements indicate that the friction velocity along ballasted track is at least twice as high as the friction velocity on the concrete surface (Deeg et al. 2008).

Quinn et al. (2010) conducted a study to investigate the causes of movement of ballast particles from their position in the roadbed. Damage to the railhead was becoming an issue, especially when the track was used by high-speed trains traveling in excess of 160 km/h. One of the phenomena observed in this study was so-called “ballast pitting,” as shown in Figure 2.24. The researchers observed that the railheads had erratic spots, probably due to the ballast rocks from the roadbed being caught in between the wheel and the rail head. Apparently, the rocks would be displaced from their initial position due to the high energy released by the passage of a high-speed train; the energy released would be high enough to allow the moving object to cause permanent damage to the rail. Moreover, voids within the ballast would be created due to the displacement of these particles. The purpose of this study was to study the pressures under the train at high speeds and determine at what level would the ballast particles start to move. A series of observations and measurements were performed on the High Speed 1 line connecting London to Folkestone. The location selected was a section of the line where trains were known to travel at nearly full speed (300 km/h). The observations were carried out in two phases. During the first phase, empirical observations to understand the wind behavior during the train passage were performed. The results of this phase provided an idea of the direction of the air flow.

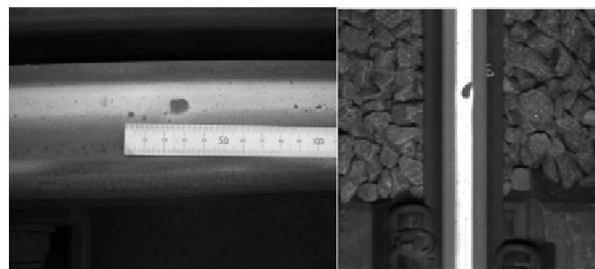


Figure 2.24: Ballast pitting damage observed on UK’s HS1 railhead (left) and from a train mounted sensor (right) (Quinn et al, 2010)

The second phase provided a quantitative measurement of the airflow underneath the train. A series of static Pitot tubes were installed on the track. The devices measured the underfloor pressures generated by the passage of 49 trains and the results were normalized to the speed and length of the trains observed. Figure 2.23 shows the pressure coefficient variation with respect to a normalized time. The data was corrected for noise interference while taking measurements and the trailing peak pressure was not reported in

full-scale measurements. These preliminary results led to a full-scale study of the aerodynamic and dynamic forces that interact with the ballast particle. Quinn et al. (2010) developed a model that attempted to measure the displacement of ballast particles from the trackbed. The setup of the field test is schematically shown in Figure 2.25.

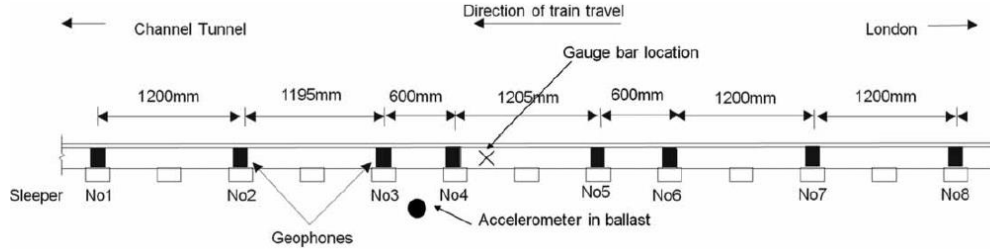


Figure 2.25: Location of the geophones used to measure the accelerations experienced by the ties and the accelerometer used to measure the accelerations of the ballast particles (Quinn et al, 2010)

The geophones measured the accelerations of the ties, while the accelerations of the particle were measured using an accelerometer embedded in the ballast bed, that behaved like a normal ballast particle. The measurements taken on the trackbed indicated an average acceleration of 7.13 m/s^2 for the ties and about half of that value for the filtered measured accelerations of the ballast particles. The unfiltered measured accelerations of the ballast showed a peak acceleration of 20 m/s^2 . Because of the very short duration of the pulse, the authors believed that the duration of the acceleration time was not enough to “lift” the ballast particle.

The experimental data collected from the field allowed the authors to develop a mathematical model for predicting the trajectories of ballast particles that are set into motion. In order to obtain a good calibration process and to obtain some meaningful data, particles up to 10 mm in diameter were chosen. The authors concluded that even though ballast particles normally have a diameter of 25 mm and above, tamping and track maintenance in general often times produce particles with a diameter less than 25 mm .

The mathematical set up of the problem can be summarized in the following “compact debris” relationships:

$$\frac{d\bar{u}}{dt} = T\sqrt{[(\bar{U} - \bar{u})^2 + (\bar{V} - \bar{v})^2 + (\bar{W} - \bar{w})]} \times (\bar{U} - \bar{u})$$

$$\frac{d\bar{v}}{dt} = T\sqrt{[(\bar{U} - \bar{u})^2 + (\bar{V} - \bar{v})^2 + (\bar{W} - \bar{w})]} \times (\bar{V} - \bar{v})$$

$$\frac{d\bar{w}}{dt} = T\sqrt{[(\bar{U} - \bar{u})^2 + (\bar{V} - \bar{v})^2 + (\bar{W} - \bar{w})]} \times (\bar{W} - \bar{w}) - 1$$

where the parameter $T = \frac{3C_D\rho U_{veh}^2}{4\rho_b Dg}$ is the Tachikawa number, $\bar{U}, \bar{V}, \bar{W}$ are the normalized air velocities, and $\bar{u}, \bar{v}, \bar{w}$ represent the normalized ballast velocities in the x, y, z directions. Using the explicit expressions for $\bar{U}, \bar{V}, \bar{W}$, which describe the mean air velocity field, the plots of the trajectories for a ballast particle of 10 mm in diameter are obtained and shown in Figure 2.26.

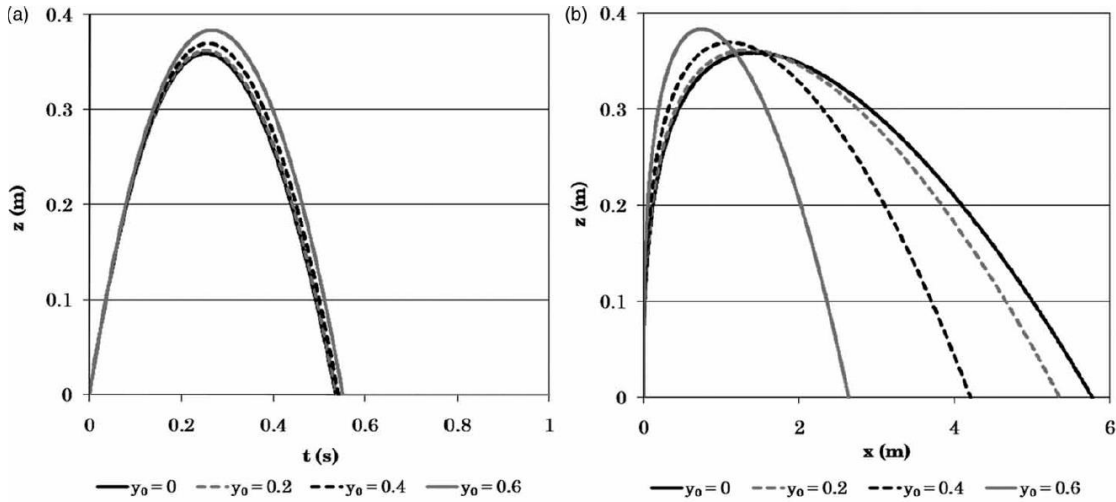


Figure 2.26: (a) vertical height time history of a 10 mm diameter particle; (b) vertical height and along track projection (Quinn et al 2010)

The value y_0 represents a different initial location of the particle across the trackbed, noting that $y_0 = 0$ m corresponds to the center of the track, while $y_0 = 0.6$ m is close to the base of the rail. It was found that in order to produce realistic trajectories, an initial speed of 2 m/s was needed. As expected, the ballast on the center-line moves furthest in this direction.

Figure 2.27 shows the paths of the particles in plan view, and it can be seen that the only particle that could jump over the rail is the one that starts to move close to the rail, i.e. $y_0 = 0.6$ m. It was noted that there is a relationship between the initial speed required for the ballast particle to jump over the rail and its particle size. Initial speeds from 1 to 3 m/s were realistic speeds, and that the likelihood of a ballast particle to displace was higher as the size of the particle decreased. However, due to the turbulent behavior of the airflow underneath the train, a stochastic approach rather than a deterministic one was recommended by the authors.

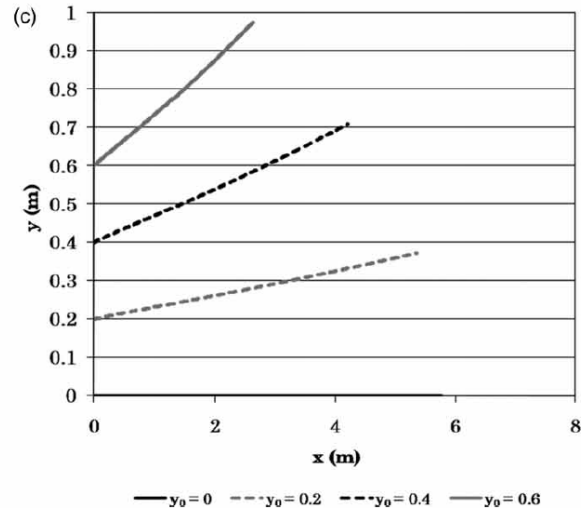


Figure 2.27: Lateral movement against along-track projection of a 10mm ballast particle (Quinn et al 2010)

Kwon and Park (2006) conducted a separate field investigation based on the results discussed in Section 2.1. Specifically, a Kiel probe array system, shown in Figure 2.28, was implemented and installed on the track to measure the flows generated by the passage of KTX trains at a speed of 300 km/h.

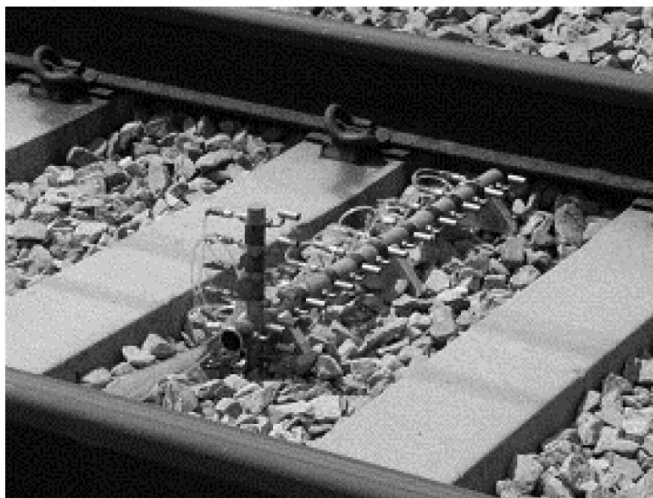


Figure 2.28: Kiel probe array installed on the Seoul-Busan High-Speed Line (Kwon and Park 2006)

The typical properties of the trains observed during the field tests are summarized in Table 2.6. The length of the KTX train was 388 m.

Table 2.6: Relevant parameters measured on the KTX train (Kwon and Park 2006)

Train no.	Measured passing time (s)	Measured Speed (km/h)	Location of fully developed flow (m)
1	4.83	289.07	37.23
2	4.80	291.08	40.83
3	4.73	295.18	29.52
4	5.00	279.43	45.11
5	4.73	295.18	49.02

To assess the magnitude of the strong wind under the train, the average wind gust \bar{U} is introduced and is evaluated by the following expression:

$$\bar{U} = \frac{300}{U_t} \int_{t_f}^{t_t} \frac{U(t)}{t_t - t_f} dt$$

where:

- t_t is the time when the tail of the train passes;
- t_f is the time when the flow is fully developed;
- U_t is the speed of the train;
- U is the velocity of the flow.

Using the above expression, the results were scaled to the speed of 300 km/h and the plots for vertical and horizontal flows are shown in Figure 2.29. The intensity of the vertical flow profile increases as it gets closer to the train underfloor while the intensity of the horizontal flow profile increases as it approaches the center of the track.

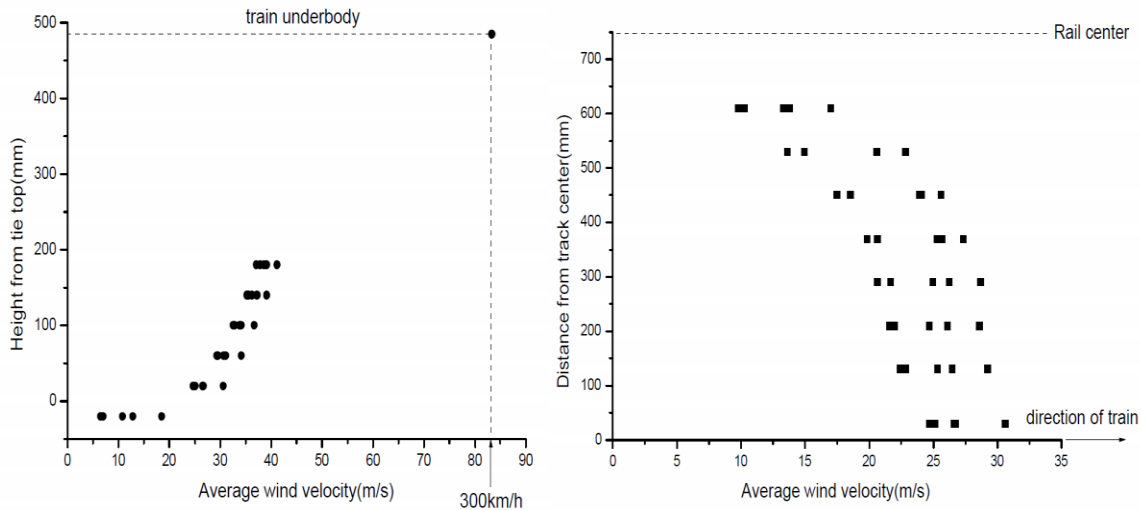


Figure 2.29: Vertical and horizontal flow velocity profiles (Kwon and Park 2006)

These results imply that the presence of the tie has a significant effect on airflow, which again indicates that a lowered ballast surface is a good mitigation strategy for ballast flying issues.

2.7 Risk Based Models

The discussion in previous sections focused on deterministic approaches, either theoretical or numerical. In this section the risk-based models from the literature will be discussed.

Kwon and Park (2006) developed a risk model based on the behavior of the ballast under high wind conditions. In this model, the Ballast Flight Probability Factor (BFPF) serves as a quantitative measure of the likelihood of ballast to fly. Introducing the concepts of minimum and maximum wind velocity at which ballast particles move (V_{min} , V_{max}), the BFPF was defined as follows:

- When the average wind velocity, V_{track} is less than V_{min} , there is no flying ballast, that is $BFPF = 0$;
- Conversely ballast will fly (certainty: $BFPF = 1$) if V_{track} is greater than V_{max} ;
- When the average wind velocity falls between the minimum and maximum value, then:

$$BFPF = \int_{m_1}^{m_2} \frac{V_{track} - V_{min}}{V_{max} - V_{min}} \frac{1}{m_2 - m_1} dm$$

Where the limits of integration represent the lower and upper mass limit of the ballast particles.

Table 2.7 shows the calculated probabilities for trains travelling at 300 and 350 km/h respectively. The mass of the ballast particle was also considered.

**Table 2.7: BFPF related to train speed and mass of ballast particle
(Kwon and Park 2006)**

Train speed	Ballast mass (g)				
	0-50	50-100	100-150	150-200	Total
300	39.80%	19.70%	11.50%	14.70%	24.20%
350	64.30%	43.30%	32.80%	33.60%	46.10%

Saussine et al. (2011) developed a risk assessment model that takes into account flow field measurements on commercial speeds, numerical development of ballast motion under an aerodynamic load using a discrete element approach, and the Stress Strength Interference Analysis approach.

For the flow field measurements, the relevant parameter to be used in this model is the global signal power, summed over the set of Pitot tubes used in field testing:

$$P_{tot} = \frac{1}{(t_2 - t_1)} \sum_{i=1}^N \int_{t_1}^{t_2} \|V(t)\|^2 dt$$

Where N is the number of Pitot tubes, V is the air flow, while t_1 and t_2 represent the time interval in which the train passes. A good correlation was found when plotting the total signal power P_{tot} and the number of displaced particles.

The Stress Strength Interference Analysis approach is an evaluation of the probabilistic interaction between two independent probability density functions. This interference can be assumed as a failure probability for the considered problem. The general framework of the methods is summarized in Figure 2.30.

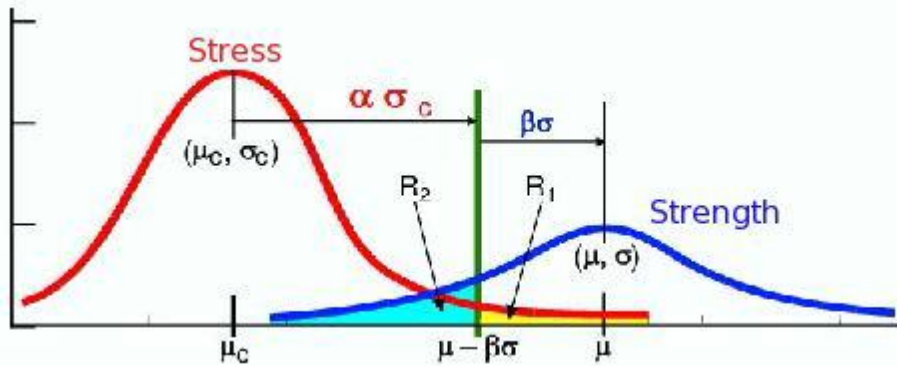


Figure 2.30: Generic Stress Strength Interface Analysis (Saussine et al., 2011)

The risk was defined by the overlapping areas of the two Gaussian distributions. Saussine et al. (2011) defined the Stress variable by the variability of the signal power and the Strength variable is defined by using the results of simulations.

Shown in Figure 2.31 are PDFs that display the signal power of various trains.

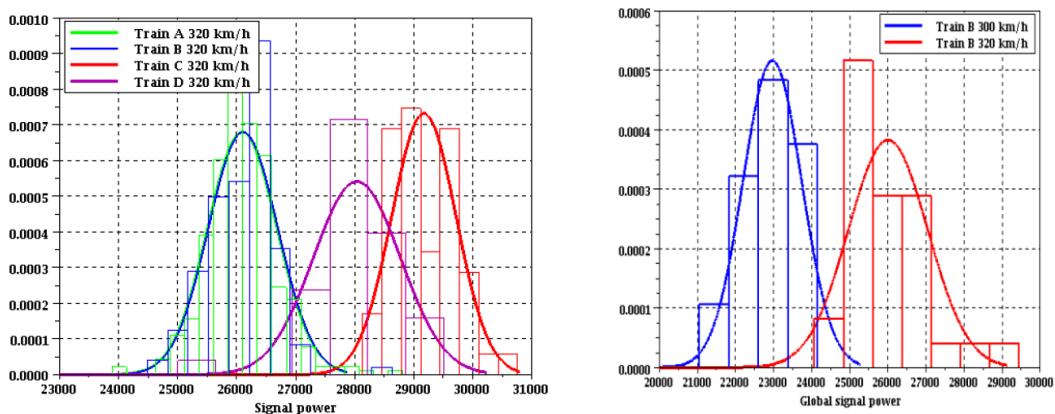


Figure 2.31: PDFs of three trains (left) and of one train at two different speeds (right) (Saussine et al. 2011)

The PDFs shown in Figure 2.31 follow Gaussian distributions. The probability and the risk were estimated using an input value of 5 and 15 ejected particles. The results are shown in Table 2.8.

Table 2.8: Calculation of the risk levels based on the number of ejected particles (Saussine et al. 2011)

Stress	300 km/h	320 km/h	Strength	Ejected grains
	22967 / 772	26000 / 1041		
Risk	5,46E-05	1,44E-02	30544 / 1800	5
	1,38E-08	8,02E-05	33848 / 1800	15

According to this model there is a higher risk of ballast flying at higher speeds.

Lazaro et al. (2011) analyzed the ballast flight phenomenon on the Madrid Barcelona high-speed line (HSL). A series of Pitot devices were installed on a portion of the HSL to measure the pressure induced by the passage of a high-speed train. The results, after the phase averaged values of wind velocity and pressure are normalized, are summarized in Figure 2.32.

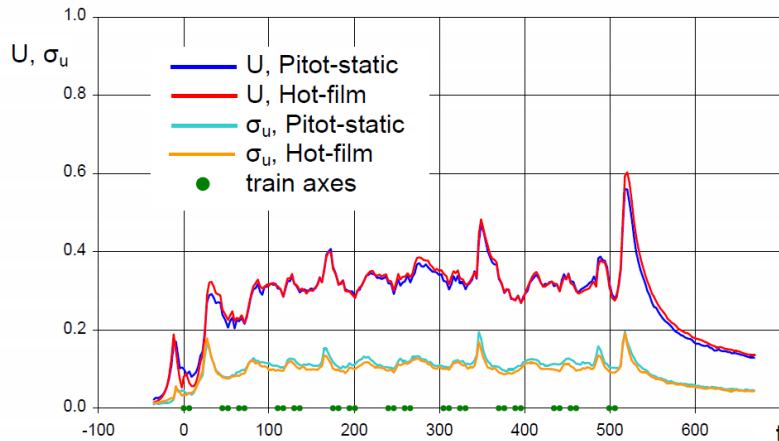


Figure 2.32: Time evolution of the phased averaged velocity (Lazaro et al. 2011)

The most important aspect of the plot in Figure 2.32 is that the initial and final peaks occurred before the train entered the point of interest and immediately after the trailing locomotive exited. From several high-speed video recordings on the high-speed line, the following stages of ballast motion were identified:

1. Induction
2. Ballast surface transport
3. Particle flight

It was found that for a given ballast density, train type, and velocity, the ballast travel distance is the inversely proportional to the particle size.

Additional results are reported in Lazaro et al. (2013). A correlation between the ballast projection risk, n_B , and the normalized velocity of trains is shown in Figure 2.33. The ballast projection risk represents the number of impacts per 100 km of swept track.

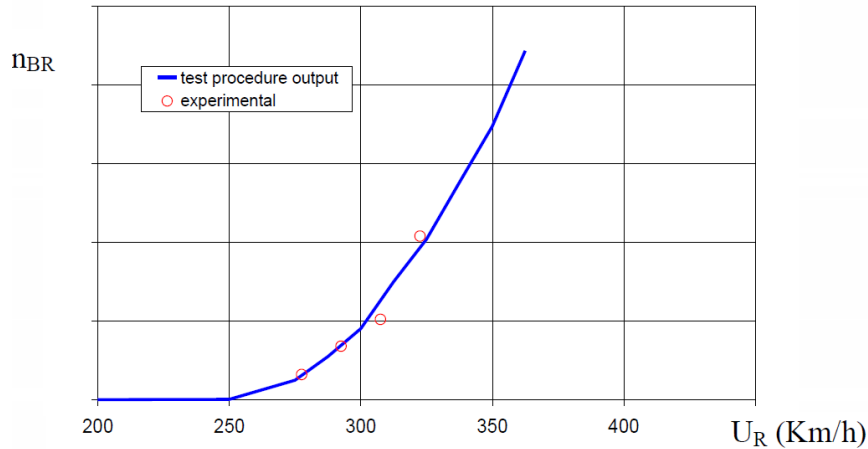


Figure 2.33: Ballast projection risk as a function of normalized train speed (Lazaro et al. 2013)

Rueter and Schroeder-Bodenstein (2008) conducted a probabilistic assessment of the ballast projection formation process. The main purpose of this work was to incorporate the main findings from several works performed under the AOA project. The simulation model proposed by the authors incorporated the following main stages:

- Initiation of ballast particle's motion
- Acceleration of ballast particle, initiation of secondary movements caused by impact, drop out from the flow field of the train
- Ballast particle reflection, disintegration of stone, absorption into the surface of the train
- Description of the flow field of the train (to be used for the motion initiation and acceleration of the ballast particle)
- Definition of track bed and ballast particle properties
- Set up environmental conditions, define the time and space routines
- Output and post processing routines

To set up the simulation, a four degree-of-freedom system was defined: translational motion of the particle in the three principal directions and rotation about the transversal axis (pitch motion). The stochastic nature of the problem was taken into account by a stochastic spread of the input parameters for each statistic variable/parameter. Stochastic events (e.g. spread in sideward motion after impact) were taken into account by random selection over parameterized distributions. This led to a Monte-Carlo approach. Random numbers were generated by the computer and setting a defined starting point of the random number vector led to deterministic, reproducible results. The results were linked to the likelihood of the ballast particles displacement. All stochastic elements of the

whole process were taken into consideration and a typical result was given in units of “amount of stones hitting the train per 1000 km”.

In the plots shown in Figure 2.34, the main results of the simulation are presented. For a 200 m long train travelling at a speed of 300 km/h, the graphs show the simulated displacement of the primary particles; the number of primary particles set into motion; the displacement of the secondary particles (or the ballast stones set into motion by impact); and the cumulative number of displaced particles as a function of time.

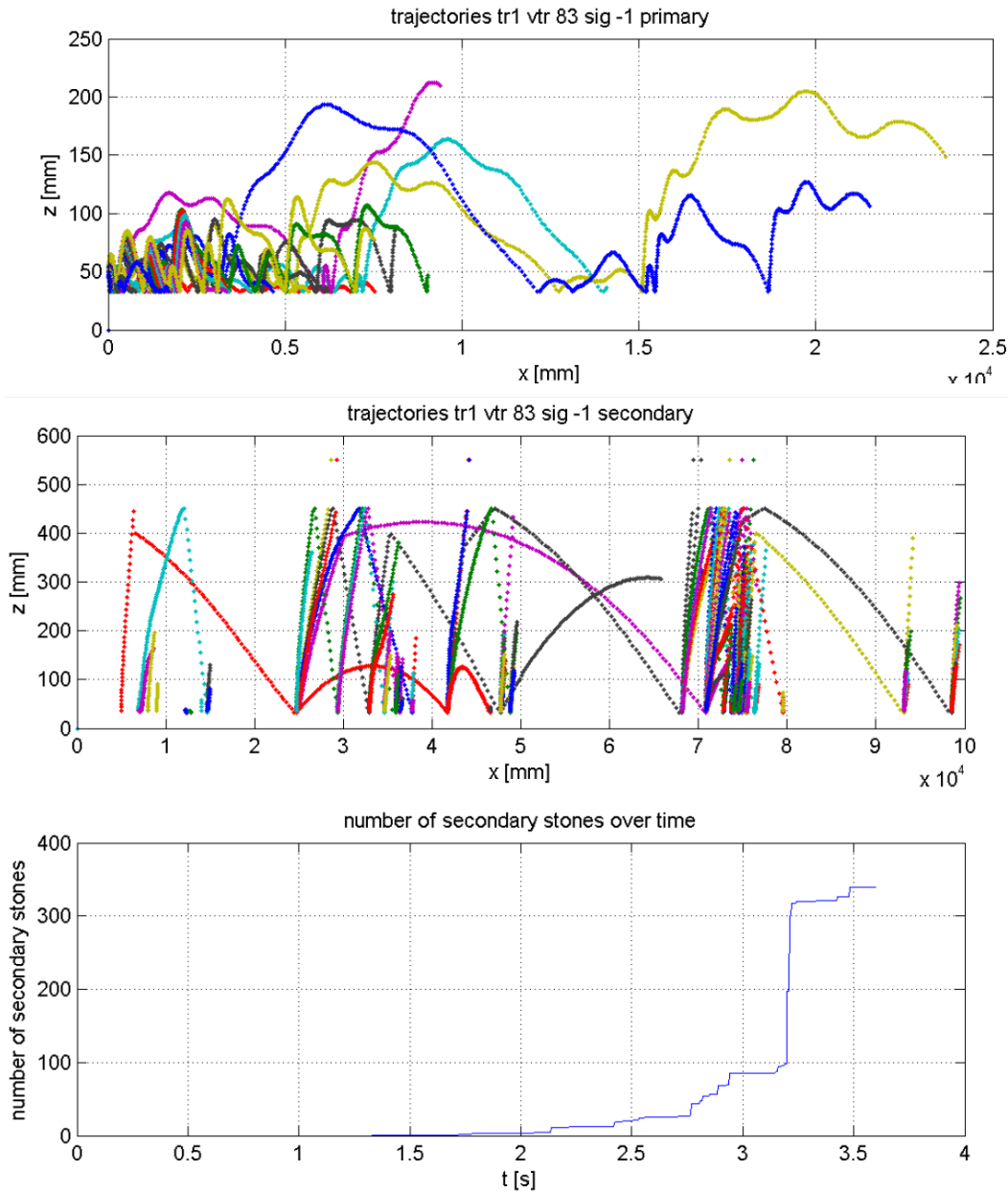


Figure 2.34: Simulated trajectories of primary ballast particles, secondary ballast particles and cumulative number of particles displaced over time (Rueter and Schroeder-Bodenstein 2008)

Parametric studies on several train configurations were also conducted. It appears that train length plays an important role with respect to the number of displaced particles. Figure 2.35 shows the number of occurrences of ballast particles displaced as a function of the train configuration studied.

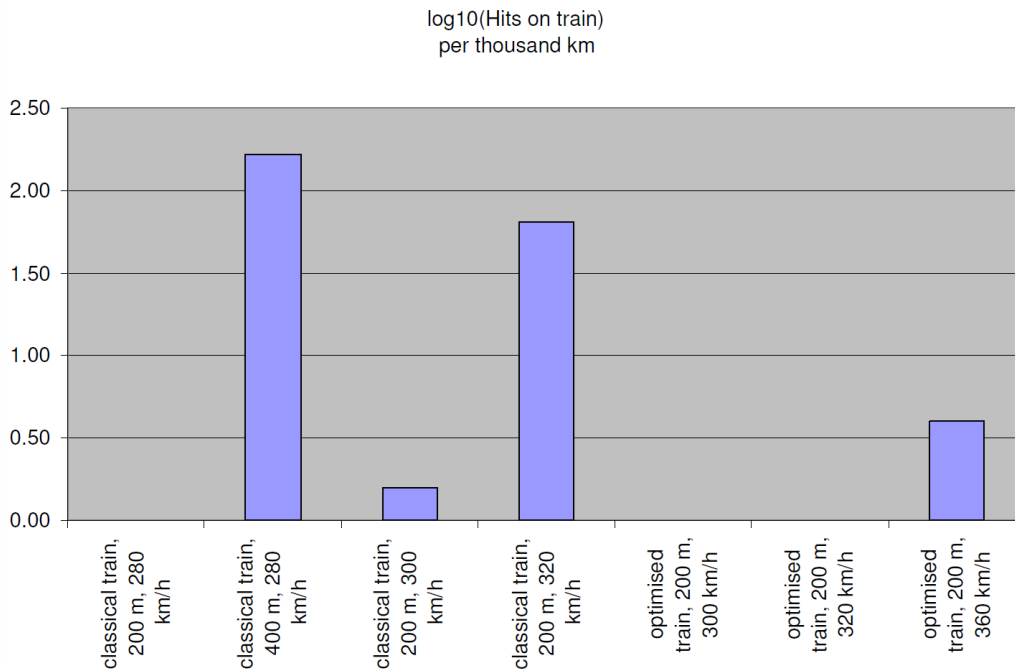


Figure 2.35: Number of ballast particle displacements (in logarithmic scale) as a function of the train configuration (Rueter et al. 2008)

Among the main conclusions of this probabilistics study is that the model does not reliably predict either ballast projection or ballast flight, due primarily to the submodels within the study’s global model. However, the study is considered as a good starting point to address the ballast projection issue. The main results reported here have been used by Lazaro (2011) in his stochastic method developed at UPM.

2.8 Other Studies

The phenomenon of flying ballast was apparently an issue known to railroad operators and manufacturers in the United States since the first half of the past century. The United States Patent office received several applications from the railroad industry seeking approval for new or improved components for use in the rolling stock or track infrastructure. Among the innovations and improvements listed in the applications was a reduction in potential damage to both rolling stock and infrastructure caused by flying ballast. The first mention of damage caused by the phenomenon can be found in an application filed in 1926 by William Wharton, Inc. for an insulated gauge rod to be used to prevent track spread (Heyl et al., 1926). It is noted in the initial description that one of

the factors that reduced the life of such rods was flying ballast. In 1937 Car Heating Company, Inc. from Chicago, IL filed a patent application for a flexible metallic hose (Van Vulpen, 1939). Again, flying ballast is mentioned as one of the reasons to file the patent. The hose's design addressed damage caused by flying ballast and other hazards.

In another example taken from US Patent Office applications, the Budd Wheel Company filed in 1945 an application to patent a new brake mechanism (Coombes, 1945). According to the specifications outlined in the document, one of the new components of the brake mechanism was designed to protect against external debris, including flying ballast, caused by the movement of the train. Other applications for both track and rolling stock improvements against flying ballast can be found in the literature both in the United States and elsewhere. Recently, a patent was filed to address damage to freight cars caused by flying ballast (Macey, 2009). Since train speeds did exceed 100 mph in the past, any occurrences of ballast flight were most likely due to the presence of small particles on top of the ties or sleepers. Another possible reason why ballast flight was mentioned in these patent applications may be that foreign objects were falling off the trains. Falling objects could include snow, ice or loose parts from the cars. If so, the flying ballast phenomenon mentioned in these patents relates rather to ballast projection caused by falling objects as opposed to ballast liftoff caused by the pressures generated by the moving train.

3 Risk Framework, Factors, and Mitigation Strategies

3.1 Risk Framework

The probabilistic occurrence of a ballast flight event can be modeled as a combination of two sub-events—the displacement of ballast particles from their rest positions and the displaced ballast particles acquiring enough momentum to experience ballast flight. Figure 3.1 shows an influence diagram that outlines the four major risk frequency factors that can contribute to the overall ballast flight risk. The chance that a ballast displacement will occur is affected by the atmospheric conditions, train aerodynamics, track responses and ground effects. If ballast displacement occurs, the possibility of ballast flight is influenced by the train aerodynamics and track responses. Potential consequences of a ballast flight event may include damage to the railhead, train body, and adjacent structures as well as injuries to maintenance workers and/or waiting passengers at through stations. The overall objective of the risk framework is to ensure that the HSR operation runs safely.

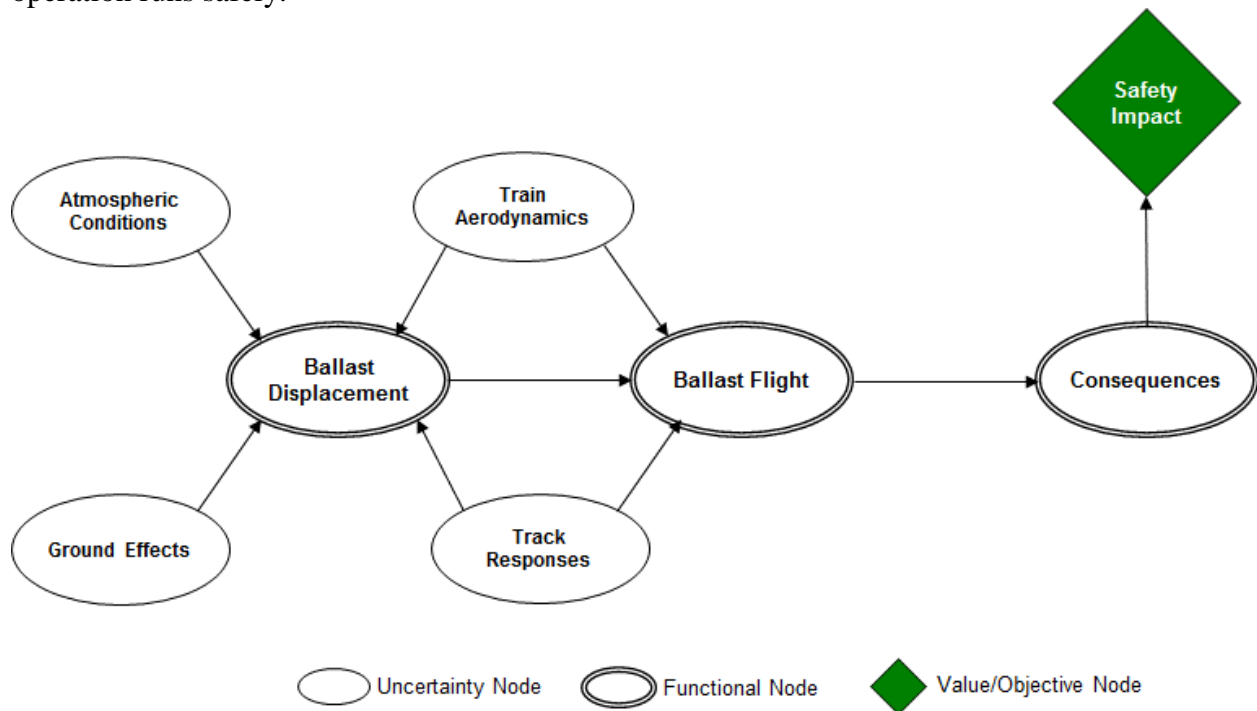


Figure 3.1: Ballast flight risk influence diagram

Risk is typically defined as a product of the likelihood or frequency of an event and the consequence of the event. Based on the conceptual understanding of a ballast flight event as described above, flying ballast risk (R_{fb}) can be defined as follows:

$$R_{fb} = P_d \times P_{fb|d} \times C$$

where P_d is the probability that ballast particles will be displaced from their rest positions, $P_{fb|d}$ is the conditional probability of a flying ballast event given the displacement, and C

is the consequence. In the following sections, the major risk factors identified in the literature review are presented and discussed in detail.

3.2 Risk Factors

3.2.1 Train Aerodynamics

Extensive studies have been conducted to understand how aerodynamic forces act on the track (Kaltenbach, 2008; Weise, 2012).

3.2.1.1 Operating speed

The key aerodynamic factor is speed (since the aerodynamic force is proportional to the square of the speed of the train). As such, speed is probably the most important contribution to ballast flight risk and HSR operators have reported that ballast flight occurrences seriously limit their ability to raise the speed on their lines. Lazaro et al. (2011) have performed a full scale experimental test to validate a risk model based on the speed of the train and the chances of ballast being displaced from its “at rest” position dramatically increased as the speed of the train went above 260 km/h (161.5 mph). Similar results were found in field studies performed in Italy (Diana, 2012; Rocchi, 2013).

3.2.1.2 Train design

The nose design of the front of a train may affect the likelihood of flying ballast. The length of the train should also be taken into account and is considered important by HSR operators when attempting to characterize flying ballast. Studies performed in Spain as well as in Italy suggested that the length of the train played a major role in the initial displacement of particles (Agretti, 2012; Lazaro, 2011). One of the best descriptors to represent the aerodynamic design of a train is the drag coefficient, c_d . Key factors affecting c_d are the train operating speed and cross sectional area. For example a conventional passenger train will have a high value of c_d , since the cross sectional area of a conventional locomotive is higher compared to that of a modern high-speed train.

3.2.1.3 Underfloor carbody design

Trains have a variety of underfloor carbody layouts. For example, old passenger cars may have units for air conditioning and water tanks installed underneath the floor without much concern about the aerodynamic effects, because the speeds of non-HSR passenger trains do not exceed 200 km/h (125 mph). With the advent of high-speed trains the aerodynamic effect gained increased importance. Newer passenger cars now present a smooth underbody to minimize the turbulence effect.

3.2.1.4 Intercar gap

The distance between two adjacent cars appears to influence the turbulence produced by the passage of the train, as noted by Saussine and Paradot (2008). The distance between the ends of adjacent cars allows air underneath the carbody to escape.

3.2.1.5 *Truck/bogie design*

The important truck/bogie element to consider is the design of the flange of the wheel. If a ballast particle is set into motion, the particle could hit the tip of the flange, thus causing the projection of the particle.

3.2.1.6 *Tunnel operation*

While the speed of 260 km/h may be a threshold value for ballast flight, other environments may lead to flight at lower speeds. For example, a tunnel can impose a boundary to the air flow generated by the train and cause flight to occur. It has been noted that in tunnels where posted speed limits were around 140 km/h (87 mph), the sign posts appeared to have significant damage from objects hitting the signs at high speeds.

3.2.2 *Track Responses*

As discussed in the literature review section, several models are available to characterize the response of the track structure to the exciting loads that are imparted by the train. These models are relatively accurate in predicting the behavior of track as a whole, but have limited ability to explain the initiating mechanisms of ballast displacements.

3.2.2.1 *Dynamic load*

Several research studies have explored the behavior of ballast subjected to the dynamic load of the train (Luo et al., 1996). It was discovered that under certain loading conditions, the particles at the surface of the track would become weightless, meaning that the reacting forces applied to the particle would be large enough to overcome gravity.

3.2.2.2 *Angle of impact*

If a displaced ballast particle hits a train, the particle is classified as a projected object. It would either impact another location of the train or the trackbed. Depending on the speed of impact and the angle of impact, this may result in a “chain reaction” where other ballast particles may be ejected from their original positions. It was found (Saussine, 2008) that the angle of impact can change the outcome of such reactions. As the angle of impact increases, the number of particles ejected from the bed appears to linearly increase (Schroeder-Bodenstein, 2008).

3.2.2.3 *Truck/bogie design amplification factor*

The distance between wheel sets and the distance between bogies can change the load input frequency to the track, thus causing the track to respond differently.

3.2.2.4 *Ballast particle mass and shape*

Typically, HSR systems require the use of the best quality ballast. Most HSR operators in the world—SNCF, RFI, and the Spanish railway administrator Administración de Infraestructuras Ferroviarias de España (ADIF) among others—require ballast to satisfy strict gradation specifications. Kwon & Park (2006) performed an analysis of ballast particles being displaced in a wind tunnel setting. They found that the size of the particle had a direct relationship with its likelihood to be picked up by winds. Specifically, the lower the ballast particle weighed, the higher the likelihood of the particle to be picked up by aerodynamic forces.

3.2.2.5 *Distance between tracks*

Saussine (2013) and Rodriguez (2013), among others, have indicated that the distance between tracks plays an important role in ballast flight. The aerodynamic crosswinds created by two trains passing in opposite directions could produce a sufficient force to lift a ballast particle. Amtrak has reported a case (FRA, 2013) which occurred when a Northeast Regional train travelling at 81 mph passed an opposing Acela train travelling at a speed of 101 mph and a closing speed of 182 mph resulted.

3.2.2.6 *Track maintenance standards*

The methods used by several railroad operators to maintain their tracks could potentially affect the possibility of ballast flight. The presence of ballast particles on the top of the crossties is believed to be an important factor in causing ballast flight. Poor and infrequent maintenance of the track increases the risk of finding ballast particles on the top of the crossties.

3.2.2.7 *Type of tie/sleeper*

The most common ties/sleeper designs used on ballasted HSR systems are either the prestressed monoblock concrete sleeper or the bi-block sleeper. The risk of ballast flight may be lower with the bi-block sleeper because the connecting steel is embedded within the ballast, as opposed to the monoblock.

3.2.2.8 *Tie/sleeper aerodynamic design*

The shape of the tie/sleeper used may affect the ballast flight phenomenon. For example, ADIF has developed a new type of sleeper as part of a project named Aurigidas (Alfonso, 2013). According to early results of tests conducted at speeds up to 320 km/h (200 mph), the rounded shape of the tie appears to mitigate the turbulent flow generated by the train's underbelly.

3.2.3 *Ground Effects*

3.2.3.1 *Sub-ballast quality*

The type of material used in the sub-ballast layer might affect the amplitude of the response of the track system. A layer made by hot-mix asphalt (HMA) presents a different response than a stabilized layer made of concrete aggregate or similar types of stabilized material. It is important to note that in North America the majority of existing railroads have a sub-ballast layer that has degraded over the course of the operation of the railroad.

3.2.3.2 *Sub-ballast layer response*

A hot-mix asphalt layer presents a different dynamic response than an unbound aggregate or other stabilized material. Furthermore, one has to consider track transitions,— which have an effect in terms of the differential settlement and change in the stiffness, leading to a different type of track response.

3.2.3.3 *Seismicity*

Small magnitude earthquakes, while not felt directly by humans, can produce an input ground motion to the ballast layer and cause some vibratory effects. The vibrations may not be visible (the ballast particle may not move), but the ballast particles lying on the top

layer of the ballast crib could become sensitive to the input ground motions sparked by the minor earthquake. Earthquakes of magnitude 3 or less normally do not cause a slowdown of operations, since there is not enough energy released to cause any damage to the track structure itself. However, the superposition of the input frequencies generated by both the train and the seismic activity, combined with the aerodynamic effects, may contribute to particle displacement.

3.2.4 Atmospheric Conditions

3.2.4.1 High wind

While several previous researchers have studied the effect of crosswinds on the body of the train, it is important to take into account the effect of those same crosswinds on ballast structure (Baker, 2013; Sima and Venkatasalam, 2013). High winds blowing on the track could alter the arrangement of the particles laying on the surface of the trackbed. This effect is particularly important with respect to smaller ballast particles present in the ballast for the reasons described previously.

3.2.4.2 Heavy rain

Rain may reduce the shear resistance of particles due to the lubricating effect of water. While this factor might not be relevant in sections of open air track, it may be important in closed environments such as long tunnels. As an example, one may consider the series of tunnels on the section of the Florence-Rome *Direttissima* high-speed line in Italy. Some of the sections of the line were built in the mid-1970s, and water will leak from the tunnel linings. Agretti (2012) has noted that ballast particles would move in the presence of trains travelling at speeds of 230 km/h at particular locations of the tunnel.

3.2.4.3 Snow and ice accumulation

While this phenomenon is not related directly to ballast flight, snow and ice accumulation on certain regions of the train may result in ballast projection. Specifically, when a train either enters a long tunnel where the temperature is higher than the current atmospheric temperature, blocks of snow or ice may fall onto the track, thus causing displacement of ballast particles. A similar effect could occur at a high-speed turnout. Since heaters installed on the turnout prevent the system from freezing, heat is radiated from the switch to the underbody of the train and in locations where high-speed crossovers are installed, the temporary temperature difference could cause blocks of snow or ice to fall off the train.

3.2.4.4 Other weather related conditions

Other weather related conditions that may affect the likelihood of ballast flight include rare, but extreme atmospheric conditions such as tornadoes, hurricanes and snow blizzards.

3.2.5 Risk Prioritization

An online survey was conducted to seek input from HSR experts in both industry and academic fields to verify and prioritize the risk factors discussed in sections 3.2.1 through 3.2.4. Figure 3.2 contains a sample of the form used to collect the responses.

PART A: FLYING BALLAST RISK FACTORS

Please rate the significance of each identified risk factors from Low to High. Select N/A if you think the risk factor is not relevant, or if you don't have sufficient information to provide the rating.

Train aerodynamics *

	Low	Medium Low	Medium	Medium High	High	N/A
Operating speed	<input checked="" type="radio"/>	<input type="radio"/>				
Train design	<input type="radio"/>	<input type="radio"/>	<input type="radio"/>	<input type="radio"/>	<input type="radio"/>	<input type="radio"/>
Underfloor geometry	<input type="radio"/>	<input type="radio"/>	<input type="radio"/>	<input type="radio"/>	<input type="radio"/>	<input type="radio"/>
Intercar gap	<input type="radio"/>	<input type="radio"/>	<input type="radio"/>	<input type="radio"/>	<input type="radio"/>	<input type="radio"/>
Truck/bogie design	<input type="radio"/>	<input type="radio"/>	<input type="radio"/>	<input type="radio"/>	<input type="radio"/>	<input type="radio"/>
Tunnel operation	<input type="radio"/>	<input type="radio"/>	<input type="radio"/>	<input type="radio"/>	<input type="radio"/>	<input type="radio"/>

Figure 3.2: Example portion of an online form used to collect data through a survey at <http://tinyurl.com/ballastflight>

Based on the survey, additional discussion, and interviews with identified key experts and collective knowledge of the team members in this project, the qualitative risk ratings of the identified risk factors were as shown in Table 3.1. High-priority risk factors that would affect the likelihood of a ballast flight event included operating speed, train design, dynamic load, track maintenance standard and high wind.

Table 3.1: Ballast flight risk factors and qualitative risk ratings

Risk Factors	Qualitative Risk Rating
<i>Train Aerodynamics</i>	
Operating speed	High
Train design	High
Underfloor carbody design	Medium
Intercar gap	Medium
Truck/bogie design	Low
Tunnel operation	Medium
<i>Track Response</i>	
Dynamic load	High
Angle of impact hitting ballast crib	Medium
Truck/bogie design amplifying vibration	Low
Ballast particle mass and shape	Medium
Distance between tracks	Medium
Track maintenance standard and frequency	High
Tie/sleeper type	Medium
Tie/sleeper aerodynamics design	Medium
<i>Ground Effect Conditions</i>	
Sub-ballast quality	Low
Subgrade quality	Low
Sub-ballast layer response	Medium
Seismicity	Low
<i>Atmospheric or Weather Conditions</i>	
High wind	High
Heavy rain	Low
Snow accumulation	Medium
Other weather related factors	Low

3.3 Consequences of Ballast Flight

A ballast flight event may have two possible outcomes. Either the particle flies and comes to rest without hitting the moving train or, if the particle hits the moving train, ballast projection occurs. The effects of ballast projection may vary from negligible to catastrophic, depending where the particle lands. The purpose of this section is to present a qualitative description of different potential ballast flight consequence levels that could be used in future risk assessment.

Negligible

After inspection, no damage to the train, track or immediate surroundings is observed or recorded.

Minor

When a train is hit by a ballast particle some minor damage to the train underfloor or bogies is noted. However, the damage is not significant enough to trigger out-of-service maintenance. Minor damages may include scratches to the carbody or small dents on

parts underneath the train. The track may experience some minor damage, for example a dent on the web of the rail or scratches on the surface of the ties.

Major

An impact which produces enough damage that the train is temporarily pulled out of service to undergo a full inspection. At this level, consequences can include flat wheels and damage to the braking system as well as damage to other components of the train. The ballast impacting the train can, in turn, be projected at a speed close to that of the train. Additionally, the particle could impact the ballast bed causing a chain reaction (Saussine et al., 2013) where other ballast particles are set into motion. The track is also affected by the magnitude of impact and the projected particle could hit the rail causing ballast pitting (Quinn et al., 2010). As an ultimate consequence, the track could be temporarily closed to perform major maintenance.

Critical

When projected ballast particles travel beyond the range of the train, they can cause damage to adjacent structures or surroundings (Agetti, 2012). Consequences at this level may include damage to structures. This fact is particularly important when the train is travelling through an urban area or a station. Injuries to people standing near the track could occur. Finally, these consequences could affect the public profile of the train operator.

Catastrophic

Fatalities occur due to ballast projection. The railroad could experience major lawsuits and major disruption of operations of its HSR service.

3.4 Risk Mitigation Strategies

This section discusses potential risk mitigation strategies to reduce the likelihood of a ballast flight event. The simplest mitigation strategy would be to reduce the speed of the trains. This solution, however, may defeat the main purpose of high-speed lines. In France and other countries where snow affects performance of the high-speed lines, there are provisions that mandate temporary speed reductions during bad weather conditions (Saussine et al., 2013).

Slab track is another mitigation strategy that addresses the problem of flying ballast at high speeds. It also brings other benefits in terms of life-cycle maintenance and performance over the lifetime of a HSR line. Despite these evident benefits, the cost of replacing ballasted track with slab track could be prohibitive. Slab track could be a solution that is discussed during the planning stages of a new high-speed line.

Lowering the ballast profile by 2 to 3 cm (0.8 – 1.2 in.) below the crosstie's shoulder is a risk mitigation strategy adopted by several countries, such as France, Italy and Spain. As discussed previously, stones that are more prone to be picked up are the ones laying on the surface of the crossties. By lowering the ballast profile, voids are created between the bottom of the rail and the top of the ballast (as shown in Figure 3.3). Air that was

compressed between the train and the track escapes through these voids to reduce aerodynamic pressure. This solution has appeared to have given good results in Italy and other countries, but in France this solution caused an increase in the tamping frequency. This could be explained by the fact that a lower ballast profile also implies a lower lateral resistance.



Figure 3.3: The effect of lowered ballast profile: ballast particles may be less exposed to ballast motion.

Ballast bagging is another risk mitigation strategy tested in Japan on those sections of the Shinkansen with ballasted track, as shown in Figure 3.4. If this solution is employed, the ballast particles are contained within the “bag” and no ballast flight can occur. However, the bags need to be removed and replaced for track maintenance.



Figure 3.4: Ballast bags placed on the Japanese Shinkansen

In Spain, ADIF has created a new type of sleeper as part of a project called Aurigidas (Alfonso 2013). The sleepers have been installed on a small portion of the Madrid – Barcelona HSL, and it appears that the aerodynamic forces felt by the trackbed are about 21 percent lower compared with that of a “regular” trackbed. This solution is still being developed.

4 Ballast Flight Risk on Current and Planned U.S. Passenger Train Systems

4.1 Background

This chapter discusses the identified risk factors related to ballast flight in current and planned passenger rail corridors in the United States. Figure 4.1 shows potential HSR corridors across the country with other existing passenger rail routes. Short and regional transit lines are not considered in this report. As of 2013, there are eleven high-speed rail corridors that have been designated by the Federal Railroad Administration (FRA, 2013). Corridors where the maximum allowable speed for passenger trains is below 110 mph will not be discussed, as the ballast flight risk is expected to be negligible.



Figure 4.1: Vision for future HSR systems in the United States

4.2 Overview of Passenger Rail Services in the United States

4.2.1 North East

Along the Central-North Atlantic coast lies the North East Corridor (NEC), a railway system connecting the major cities of Washington, New York and Boston. The routes that constitute the current corridor were built during the 19th century. The corridor has undergone a major upgrade during the 1990s to provide high-speed service. Much of the

line is built for speeds higher than the 79 mph generally permitted for typical passenger train operations. This allows Amtrak to operate higher-speed rail services, such as the intercity Northeast Regional and Keystone Service trains that go up to 125 mph, as well as North America's only high-speed train, the Acela Express, which runs up to 150 mph on several sections in Massachusetts and Rhode Island. In 2012, Amtrak performed test runs at Trenton, NJ in order to increase the trains' top speed to 165 mph.

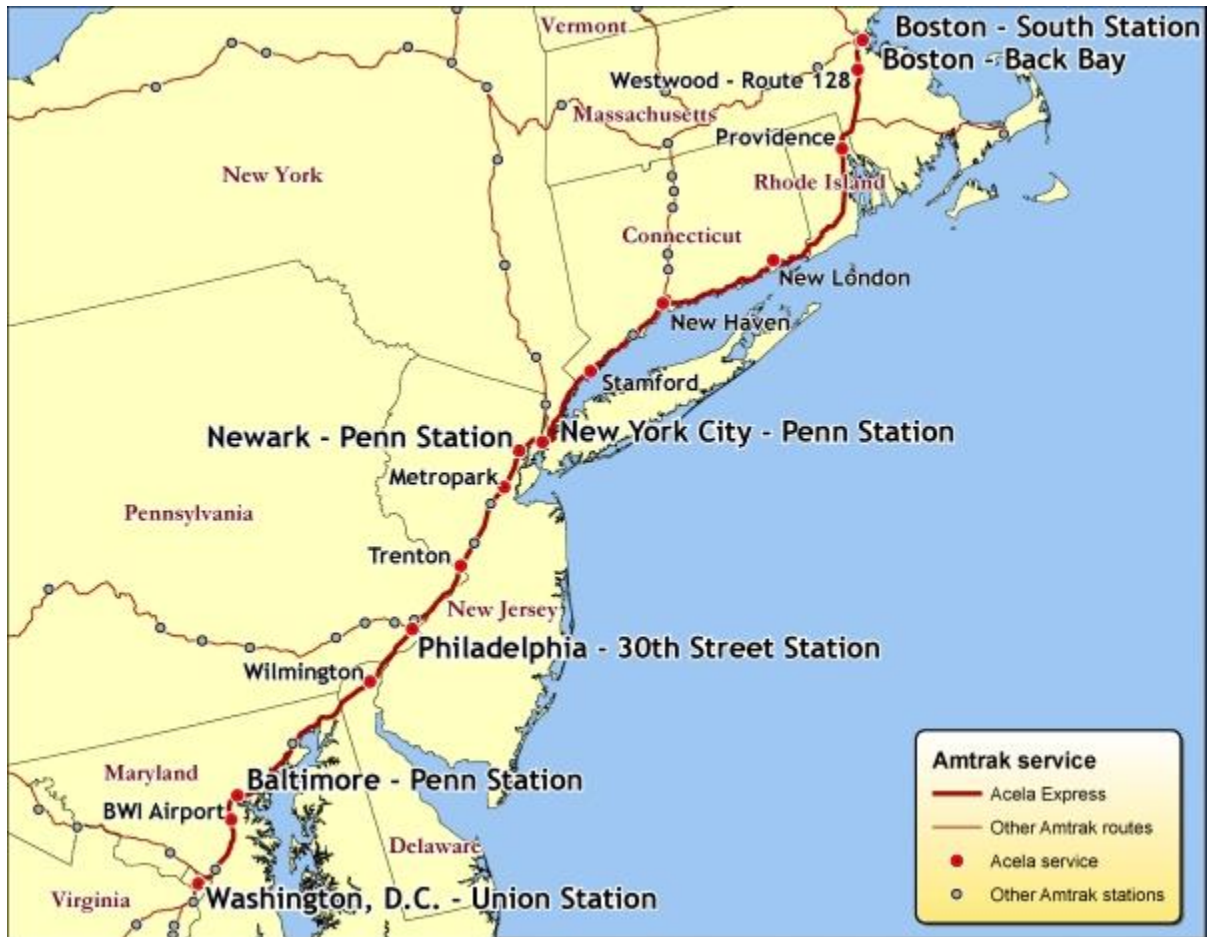


Figure 4.2: The North East Corridor (www.amtrak.com)

Amtrak plans to improve the alignment along the corridor and acquire new trainsets that could be operated at 186 mph. In the second stage of its plans, a so-called “next gen” NEC would be developed and trains would travel at 220 mph. This future phase includes a new track alignment to follow the current NEC route (Amtrak 2012).

The Keystone Corridor connects the cities of Philadelphia and Pittsburgh. The section between Philadelphia and Harrisburg has been electrified while diesel locomotives serve the remaining portion of the route. The electrified section offers train service at 110 mph. The remainder of the line is currently being studied for possible electrification. According to the Pennsylvania Department of Transportation there are plans to seal the corridor by eliminating the remaining grade crossings, thus allowing service at 125 mph.

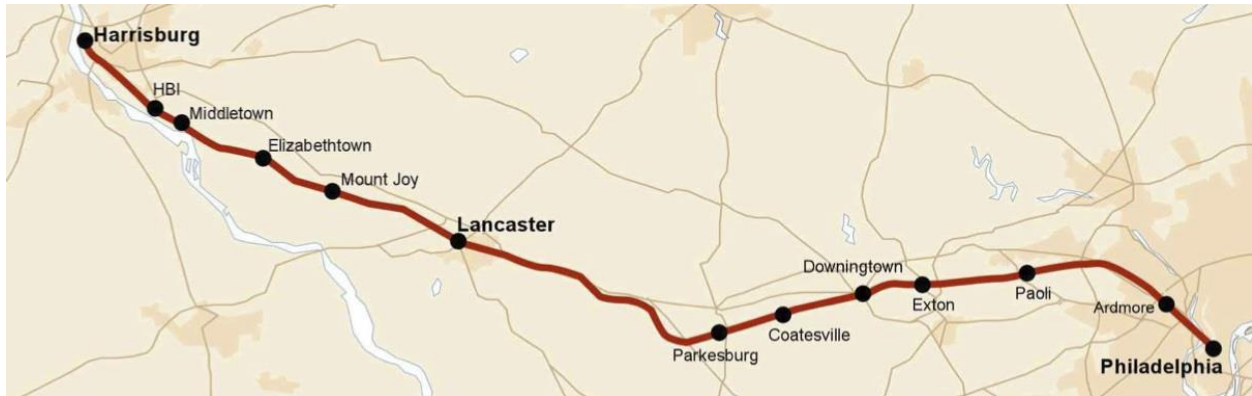


Figure 4.3: The Keystone Corridor

The Empire Corridor runs across the state of New York connecting the cities of New York, Albany, Syracuse, Rochester and Buffalo. The Department of Transportation of New York State is conducting a Tier 1 Environmental Impact Statement (EIS) with the goal of improving rail service along the corridor by allowing service at 125 mph. The traffic will be a mix of passenger and freight trains.

4.2.2 South East

The South East Corridor can be regarded as a continuation to the south of the North East Corridor. The proposed plan envisioned by the Departments of Transportation of the states involved is an incremental upgrade of passenger service from the current 79 mph to 110 mph.

Recently a study has been released by the State of Georgia, which was funded in part by the Georgia DOT and in part by private funds. Three alternatives were evaluated. The first one considers rehabilitating portions of abandoned railroad right-of-ways (ROWs) and existing portions of railroad, reconstructing the trackbed where needed, and preparing the route for 110 mph operations. The second and third alternatives would median of the Interstates 185/85 from Columbus to Atlanta. While the second alternative would use diesel power, thus producing speeds up to 125 mph, the final alternative considered would include electrification and trains operating at 150/200 mph (Ledger Inquirer, 2014).

The State of Florida proposed a project consisting of a new railway system that would initially connect the cities of Tampa and Orlando using the median of Interstate 4. Planned speeds were up to 170 mph. The project would have been subsequently extended from Orlando to Miami. According to the latest design plans, the track was to be ballasted. Although the project was cancelled in 2011, some private initiatives are being pursued. The Florida East Coast Railway (FEC) is pursuing the implementation of a passenger service named All Aboard Florida.



**Figure 4.4: Schematic route of the service from Miami to Orlando
(All Aboard Florida, 2014)**

The proposed service will be owned, operated, and maintained by FEC, and it will establish a higher-speed passenger service between Miami and Orlando. The track between West Palm Beach and Cocoa will allow 110 mph operations, while the track from Cocoa to Orlando will allow 125 mph operations. Currently, the project is at its EIS stage, and a Record of Decision is scheduled to be issued by the FRA in April 2014. Most of the alignment considered is a 100-year-old railroad that will undergo improvements to meet the FRA class 6 and 7 standards (All Aboard Florida, 2014).

4.2.3 Midwest

When the Chicago-St. Louis incremental upgrade is completed, it will allow passenger service at 110 mph from the city of Joliet to East St. Louis. In 2009, the Illinois Department of Transportation (DOT) received \$1.1 billion in ARRA funds to carry out corridor wide improvements. Tasks included a complete renovation of the track structure from East St. Louis (Q Tower) to south of Joliet (UD Tower). Several curves have been realigned to allow operating speeds of between 90 and 110 mph. Currently, 110 mph

service is offered on two Amtrak trains between the cities of Dwight and Pontiac, IL. According to the Illinois DOT, a full build-out phase is planned once the existing infrastructure improvements for the current track configuration are complete (e.g. stations, Positive Train Control implementation among others). The full build-out will consist of a second main track installation, improvements on the selected alternative from Chicago to Joliet, and relocation of both freight and passenger service in the city of Springfield from its current location to a new designated corridor on the east of the city. Currently the full build-out is under environmental review. Figure 4.5 shows a schematic outline of the route.

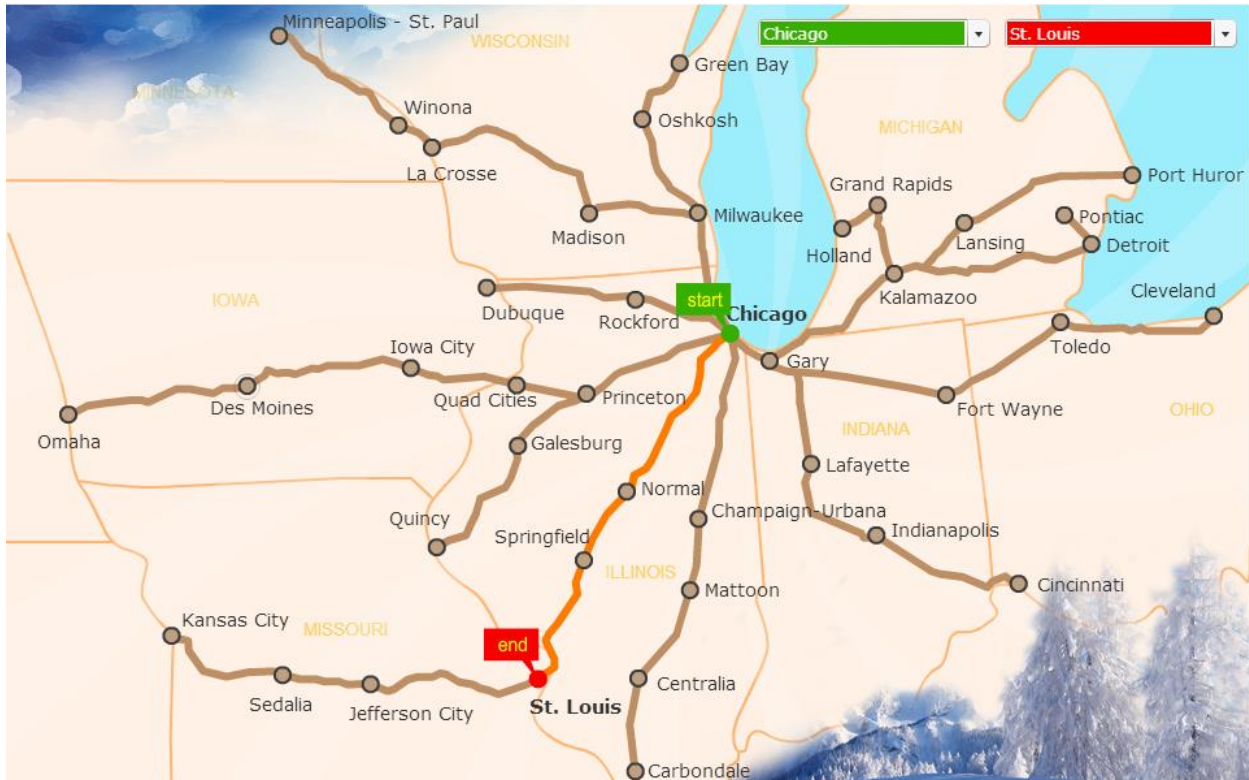


Figure 4.5: The route for Chicago to St. Louis (Midwest High-Speed Rail, 2014)

The route is all surface and no tunnels are present on any part of the corridor. Several grade crossings are present, although improvements are being implemented by means of installing four quadrant gates.

The Iowa DOT has carried out a Tier I EIS to assess the impacts of upgrading a corridor connecting Chicago to Council-Bluffs Omaha, Nebraska. The EIS proposed four possible alternatives to the FRA, and the FRA issued in August 2013 a Record of Decision (ROD) stating that that alternative 4-A met the requirements for Project Needs and minimized impact to the environment (FRA-Iowa ROD, 2013). The proposed alignment is shown in Figure 4.6.



Figure 4.6: Proposed alignment of the Chicago-Omaha corridor (FRA-Iowa ROD, 2013)

The Iowa DOT plans to implement the corridor by stages. Current passenger service requires over 9 hours to cover the distance between Chicago and Omaha. When the new service is completed, it will cover the distance in less than 7 hours for 500 miles of line. The line will be a two main track running on planar support. No tunnels are envisioned. The service will be fully operational by 2040.

In 2012, the University of Illinois conducted on behalf of the Illinois DOT a preliminary feasibility study to assess the possibility of building a true high-speed line connecting the cities of Chicago, St. Louis, and Indianapolis. Of the several route alternatives considered, some in which the main infrastructure would be ballasted track. The alignments considered would allow speeds up to 220 mph. One of the alignments studied would use interstate medians as a possible roadbed for the main track.

The Chicago – Kalamazoo – Detroit Corridor (Figure 4.7) is the second main passenger route in the Midwest region that is being upgraded to allow 110 mph operations. Current service allows 110 mph speeds from Porter, IN to Kalamazoo, MI. Most of the alignment is single-track with plans in the future to introduce segments of 10-20 miles in length of second main track. The length of such sections would allow train meets/passes at high speeds (Franke, 2014).

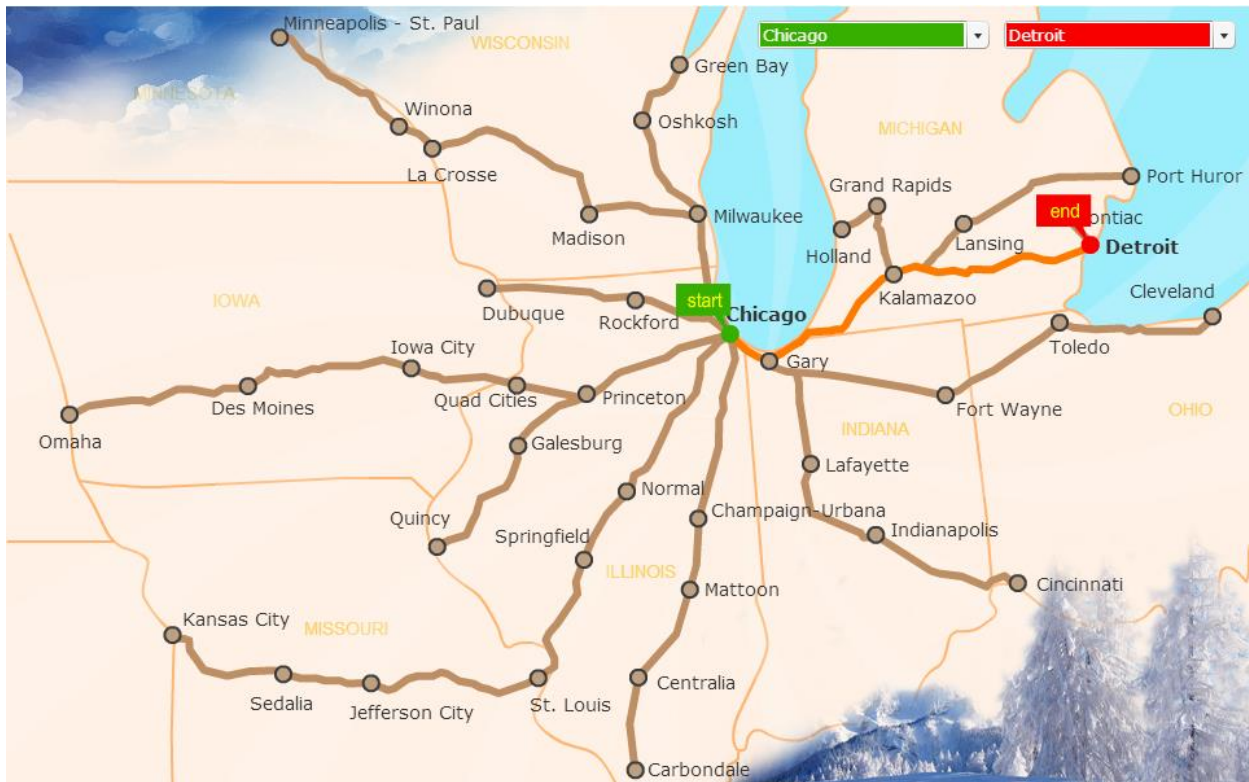


Figure 4.7: Route of the Chicago-Detroit corridor (Midwest High-Speed Rail, 2014)

4.2.4 West

The Pacific Northwest Corridor is the longest railroad considered by the FRA as a designated HSR corridor. Speeds along this line will reach 110 mph at the completion of the improvements. Although several short tunnels are present along the route, the speed at these locations is much lower. All tunnels are single or double track with reduced speeds due to either curvature geometry or proximity to stations (Caughron, 2014).

The California High-Speed Rail system is currently in its final phases of design and the first section in the Central Valley is scheduled to start its construction in 2014. The system will allow speeds up to 220 mph. On those sections, however, the track structure is planned to be slab rather than ballasted. According to later project developments, the system will share track with existing freight lines and the high-speed trains will travel at the speed set by the host railroad.

4.3 Relevance of Key Ballast Flight Risk Factors

4.3.1 Operating Speed

In corridors where the current or planned operating speed is 79 mph or less (up to track class 4), the risk of ballast flight is very low. A small risk could arise if the train enters a

tunnel where the authorized speed is 79 mph. The pressure waves and turbulent flow generated in the tunnel might create the conditions for ballast particles to be set into motion. As an example, DB has had cases where trains travelling at similar speeds produced some damage to wayside sign posts installed on the walls of the tunnels.

On corridors where the maximum allowed speed for passenger trains is 110 mph, the risk of ballast flight is expected to be medium low to medium. However, this risk is highest when trains meet and pass each other at their maximum speeds. The trains' combined speed could be up to 220 mph and the distance between tracks plays a key role. The turbulence generated by the trains when they pass one another is enough to create the appropriate conditions for ballast particles to be displaced. This risk would increase in locations where a secondary station is present.

On the NEC, current train speeds range from above 79 mph to 150 mph. Future speeds above 160 mph would be enough to trigger the motion of ballast particles present on top of the ties. The combined speed of two Acela trains further increases the risk of ballast flight. This is particularly true at locations such as secondary stations, or at locations where the distance between tracks is 13 or 14 feet. There was a ballast flight incident recorded on the FRA accident database (FRA, 2003) where an Acela travelling at 101 mph passed a Northeast Regional travelling in the opposite direction at 81 mph. The combined speed was 182 mph and a ballast particle was lifted by the consequent turbulent flow of the air.

On true HSR lines, the risk of ballast flight increases with the square of the speed of the train (Lazaro, 2011). Currently, no true HSR systems exist in the United States. As of 2013, the only active HSR project is in California. The project includes slab track on the main line, while ballasted track will be used on the sections of the proposed alignment to be shared with existing railroads. There is no ballast flight risk for sections with slab track. A medium to medium-low risk is expected on ballasted sections where a shared track or shared ROW is planned. The proposed operating speed for future true HSR systems would be a relevant risk factor when considering ballast flight.

In addition, a true HSR system in the US might use interstate medians for the ROW. For example, the Florida HSR project had considered using the I-4 median for its ROW. If medians are used, there is a high risk from ballast flight due to the proximity of the railway to the highway vehicles.

4.3.2 Train Design

The design of the train impacts the probability of ballast flying. For example, the intercar gap studied by Saussine and Paradot (2008) appears to change the likelihood of ballast particles being picked up. The drag coefficient associated with each type of train also plays a key role. The airflow generated by the passage of the train changes as the shape of the train changes. If high-speed trains are employed on shared corridors (where speeds are up to 125 mph), the risk of flying ballast may be affected by the aerodynamic profile of the locomotive and the intercar gap.

Diesel rolling stocks capable of reaching such speeds are in the process of being built in the United States. Recently, the Illinois Department of Transportation issued a letter of intent to purchase approximately 35 high efficiency Siemens diesel locomotives, which are capable of reaching speeds of 125 mph. The locomotives will be distributed among the States of Illinois, Missouri, California, Michigan and Washington.

4.3.3 Dynamic Load

The high-speed trains that are currently used in Europe and Asia are made up as either distributed motorized units or head/tail locomotives.



Figure 4.8: The TGV and ICE 3 HS trainsets (<http://4rail.net>)

The axle load of high-speed trains can vary between 13 tons (Alstom AGV) to 17 tons (ETR 500, power unit). Each train design has its unique wheel arrangement, which in turn places a different input dynamic load on the track. While the effect of dynamic load on shared corridors presents a low risk of ballast flight, the risk increases in those locations where speeds are in excess of 150 mph. Such speeds (for example, in sections of the NEC where the Acela service is authorized to travel at 150 mph) are close to the critical speeds that could match Raleigh waves along the subsoil. The hazard is the resonant effect created by the passage of the train. In such situations, ballast particles at the surface of the ballast bed could experience a weightless state long enough to be lifted by the turbulent effect of the passing train.

4.3.4 Track Maintenance Standard

Out of all the situations where ballast can be set into motion, the majority of HSR operators believe that ballast flight is most likely to occur at the top of the tie/sleeper. According to guidelines set forth by HSR operators (SNCF and RFI among others) the sleepers must be free of ballast particles on their surface. As a result, track maintenance plays a direct role in the level of hazard for ballast flight.



Figure 4.9: Example of HS track where no ballast particles are present on top of the sleepers.

Most of the time, no sweeping is performed after the stabilization or resurfacing of the track and ballast particles end up lying on the surface of the sleeper. Incidences of ballast flight were reported when the first HST passes on the maintained track (Saussine, 2013). Subsequent passes did not observe ballast flight, since the ballast particles that were present on top of the sleepers had been swept away. The need to clean ballast particles from sleepers should be carefully considered especially on those lines where speeds are in excess of 160 mph.

4.3.5 High Wind

The Midwest is a region of the United States where high-wind conditions occur frequently. In the springtime and in those days with temperatures much higher than the norm, extreme atmospheric conditions may occur such as tornadoes or strong wind gusts in excess of 70 mph. On railway lines where speeds are 110 mph and above, the combination of the turbulence effect with the presence of high wind may create the conditions of ballast motion.

4.4 Risk Screening Tool

The University of Illinois has developed a risk screening tool that evaluates the ballast flight risk at any specific section along a rail network. It can be used to compare the relative ballast flight risk at different locations on a current or future planned HSR system. The tool will assist in prioritizing risk mitigation implementations, if needed, along a specific HSR system.

The compact version of the risk screening tool, which is described in detail in this section of the report, considers the five major risk categories identified through the literature review. The complete version considers all the risk factors identified in the literature review, and is summarized in Table 3.1. Figure 4.10 contains a screenshot of the compact version.

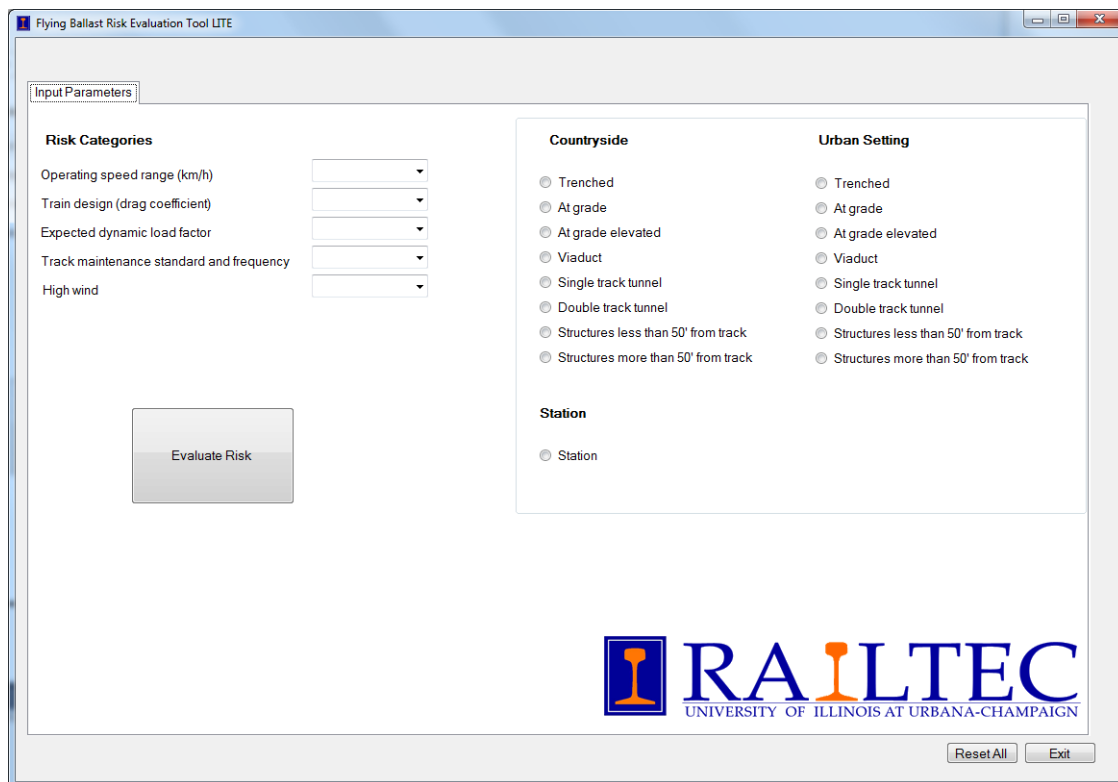


Figure 4.10: The Flying Ballast Risk Evaluation Tool, Compact Version

The five major risk factors included are:

- Operating speed
- Train design
- Expected dynamic load
- Track maintenance standard and frequency
- High wind

A qualitative score has been assigned to each of the key factors. The following discussion addresses the score assignment in detail.

4.4.1.1 Operating speed

As the speed of the train increases, the risk associated with ballast flight increases. The risk evaluation tool uses speed ranges to account for intermediate speeds, where the risk of flying ballast does not appear to change significantly. For example the range 150-200 km/h accommodates the speed of 176 km/h (110 mph). Such speed presents risks that are still within the range of the low and high proposed end. The tool also includes speeds beyond the current operating speeds to accommodate future train operations.

Table 4.1: Qualitative severity score for operating speed ranges

Operating Speed (km/h)	Score
150-200	1.1
200-250	1.2
250-300	1.3
300-350	1.4
350-400	1.5
400-450	1.6
450-500	1.7
More than 500	1.8

4.4.1.2 Train design

The design of the train affects the track behavior as discussed in the literature review. For example an ICE 3 train produces a different effect to the track compared to a TGV train. The governing aerodynamic parameter is the drag coefficient. In the tool, ranges of drag coefficients have been included. A low score is assigned to the lowest ranges, while the higher drag coefficients are assigned a high qualitative score.

Table 4.2: Qualitative severity score for train design (drag coefficient)

Train Design	Score
Less than 0.01	1
0.01-0.05	1.2
0.05-0.08	1.3
0.08-0.1	1.4
0.1-0.5	1.5
More than 0.5	1.6

4.4.1.3 Expected dynamic load

According to typical design standards (Italferr MPE, 1992, among others), the static load of any given train is not the actual load experienced by the track. A factor is introduced to quantitatively measure the actual load on the track. The American Railway Engineering and Maintenance of Way Association uses a formula to describe the dynamic load felt by the track when a train passes at any given speed. Other countries have developed their own methodology to assess a factor that is applied to the static load of the heaviest rolling stock when designing the track.

The tool incorporates the dynamic factors used on Italian HSR design, ranging from 1.2 to 1.8. Since the dynamic load has a direct relation with the speed of the train (Hay 1982),

a low score is assigned to a low dynamic load factor. A high score is assigned to a high dynamic load factor.

Table 4.3: Qualitative severity scores for the expected dynamic loads

Expected Dynamic Load	Score
Less than 1.2	1
1.2	1.2
1.4	1.3
1.6	1.4
1.8	1.5
More than 1.8	1.6

4.4.1.4 Track maintenance standard and frequency

The quality of the track upon which a train runs plays a fundamental role in the overall quality of the train ride felt by the passenger. Well-maintained track requires a high maintenance standard, and, in the case of ballasted HSR, high-frequency maintenance as well. An indicator of good quality maintenance is the absence of ballast particles from the top of the ties/sleepers. This tool uses the following standards of maintenance:

- Very poor and rare: “Very poor maintenance” means that little work is done in order to maintain an acceptable quality of the track; in addition, the maintenance is done rarely at irregular intervals, no more than once every six months. The quality of the track is barely acceptable with some degradation on the track structure, such as cracked ties or serious rail defects. A high score is assigned to this scenario.
- Poor and rare: The maintenance standard is somewhat better compared to the previous scenario; the frequency is still up to once every six months, but the quality of the track is better compared to the previous scenario. Examples would be better ballast quality, ties are in acceptable conditions, and particles of ballast often appear on top of the tie. A medium to high score is assigned to this scenario.
- Regular: The track is maintained at regular intervals, once every three months. The quality of the track is acceptable, although ballast particles may be present on top of the ties. A score of medium is assigned to this scenario.
- Frequent and good: The track is maintained at a high frequency in order to maintain the highest quality and maintenance is done on a monthly basis. The track structure appears to be in optimal conditions with little or no presence of ballast particles on top of the ties. A score of low is assigned to this scenario.

Table 4.4: Qualitative severity score for track maintenance

Track Maintenance Standard	Score
Very rare and poor	1.5
Rare and poor	1.4
Regular	1.3
Frequent and good	1.2

4.4.1.5 High wind

High-speed lines may run in locations where frequent wind gusts may occur. A low score is assigned to those regions where high winds are not likely to occur and a high score is assigned to locations where high winds are most likely to occur.

Table 4.5: Qualitative severity score for high wind

High Wind	Score
Low intensity	1.1
Medium intensity	1.3
High intensity	1.5

4.4.1.6 Location of the track of interest

The tool allows the user to select the location of the track where risk is assessed. It provides a countryside setting, an urban setting and a station. Both the countryside and urban settings contain the same set of track configurations (on a viaduct, at grade, near or far from adjacent structures, or on elevation). Each track location carries a numerical score related to the consequence level of flying ballast. For example the selection of countryside “at grade” will carry a consequence level of 1.2, since there is little risk associated with the phenomenon of flying ballast. The station scenario carries the highest score (1.5) related to consequence level. Such a high value is due to the presence of people on the platforms of the station. These people would be exposed to the hazard of being hit by a ballast particle airborne from the track during the passage of the train.

Table 4.6: Qualitative score for countryside consequence levels

Countryside	Consequence level
Trenched	1.2
At grade	1.2
At grade elevated	1.3
Viaduct	1.3
Single track tunnel	1.2
Double track tunnel	1.3
Structures less than 50' from track	1.5
Structures more than 50' from track	1.4

Table 4.7: Qualitative score for urban consequence levels

Urban setting	Consequence level
Trenched	1.2
At grade	1.2
At grade elevated	1.3
Viaduct	1.4
Single track tunnel	1.2
Double track tunnel	1.3
Structures less than 50' from track	1.5
Structures more than 50' from track	1.4

4.4.1.7 Risk evaluation

Table 4.8 summarizes the quantitative weights identified from the survey conducted as part of this research study. The weights are normalized to the highest level assigned, 5.

Table 4.8: Normalized weights of major risk factors

Risk factors from survey	Weight from survey	Normalized Weight
Operating speed	4.71	0.942
Train design	3.71	0.742
Expected dynamic load	3.25	0.650
Track maintenance standard	3.83	0.766
High wind	2.14	0.428

Each normalized weight is then multiplied by the qualitative score assigned by the user in the tool, thus producing the weighted frequency of the particular factor considered. The

sum of the weighted frequency is then multiplied by the consequence level assigned by the user, thus producing the overall risk score.

5 Summary and Conclusions

This report introduced the phenomenon of flying ballast, identified key risk factors and assessed the qualitative risk of the phenomenon in the United States. Ballast projection has been a known issue to both freight and passenger rail operators. Flying ballast has been examined extensively with the implementation of high-speed lines on ballasted track. A comprehensive literature review has been carried out, in order to understand the relevant work done to understand the phenomenon. A set of key risk factors was identified and assessed for relevance to current or planned high-speed and passenger rail systems in the United States. A qualitative hazard assessment method has also been developed using a simple software tool that incorporates the five most relevant risk factors of flying ballast: operating speed, train design, dynamic load, track maintenance and high wind.

Flying ballast is a phenomenon that may be considered as a high risk for ballasted high-speed lines in North America. Higher speed corridors may also present a moderate level of risk of flying ballast when the appropriate conditions are met. Such conditions may include tunnel operations, snow accumulation and passing high-speed trains from opposite directions.

It is recommended that further research on the subject should be considered, especially when considering that high-speed lines will be eventually built. Research tools could include, but are not limited to, computer modeling and field tests in a closed environment.

6 References

- Agretti, M. (2012, 14 January). Sollevamento del Ballast sulla linea AV Roma-Napoli. (F. Bedini Jacobini, Interviewer).
- Alfonso, F. (2013, January 28). Una traviesa intelligente protegge al AVE del rebote de las piedras de la via. *El Economista*, p. 22.
- All Aboard Florida, <http://www.allaboardflorida.com>. Accessed 4 January 2014.
- Baker, C. (2013). Some considerations of the cross wind overturning problem. *International Workshop on Train Aerodynamics*. Birmingham.
- Claus, P. (2008). Overview of past ballast projection incidents. *Aerodynamics in Open Air* (pp. 77-82). Munich: DEUFRAKO.
- Coombes, J. H. (1945). Brake mechanism. *U.S. Patent No. 2,382,543*.
- Deeg, P. (2013, 9 April). Possible flying ballast in tunnels at low speeds. (F. Bedini Jacobini, Interviewer).
- Deeg, P. Jonsson, M.; Kaltenbach, H.J.; Schuster, P.; Weise, M. (2008). Flow speed measurement near the trackbed under passing ETR 500 Train. *Aerodynamics Open Air* (pp. 11-16). Munich: DEUFRAKO.
- Diana, G., Rocchi, D., Tomasini, G., Schito, P., & Premoli, A. (2013). Full scale experimental analysis of train induced aerodynamic forces on the ballast of Italian high speed line. *International Workshop on Train Aerodynamics*. Birmingham.
- Federal Railway Administration (FRA) Office of Safety Analysis. "Download Data on Demand," <http://safetydata.fra.dot.gov/OfficeofSafety/default.aspx>. Accessed 4 November 2013.
- Federal Railway Administration (FRA) Rail Network Development. "Completed Environmental Reviews," <https://www.fra.dot.gov/Page/P0212>. Accessed 16 January 2014.
- Franke, M. (2014, 4 January). The Chicago-Detroit HrSR corridor improvements. (F. Bedini Jacobini, interviewer).
- Garcia, J., Crespo, A., Alonso, I., (2008). Trackbed modeling with the equivalent roughness concept. *Aerodynamics in Open Air* (pp. 29-32). Munich: DEUFRAKO.
- Hay, W.W. (1982). *Railway Engineering*, John Wiley & Sons.

- Heyl, H. F., Hulbert, W. G. (1926) Insulated gauge rod. *U.S. Patent No. 1,585,495*.
- Hines, C. M. (1951). Circuit integrity indicating system. *U.S. Patent 2,573,442*.
- Italferr (1992). Manuale di progettazione esecutiva.
- Iowa Department of Transportation (2014).
<http://www.iowadot.gov/iowarail/passenger/proposedrail.html>. Accessed 16 January 2014.
- Johnson, L. L. (1961). Dust guard and seal for railroad car journal boxes. *U.S. Patent No. 2,995,389*.
- Kaltenbach, H. J. (2008a). Implications for the definition of a common measurement procedure. *Aerodynamics in Open Air* (pp. 17-19). Munich: DEUFRAKO.
- Kaltenbach, H. J. (2008b). The generic underfloor geometry laboratory experiment “BIAC”. *Aerodynamics in Open Air* (pp. 21-26). Munich: DEUFRAKO.
- Kaltenbach, H. J., Deeg, P., & Eisenhauer, M. (2008). Experimental investigation of particle dislodgement in scale 1:10 (SUMKA). *Aerodynamics in Open Air* (pp. 99-104). Munich: DEUFRAKO.
- Kirk, W. B. (1963). Brake beam with integrally formed brake cylinder. *U.S. Patent No. 3,088,550*.
- Kundu, P.; Cohen, I. (2008). Fluid Mechanics, Fourth Edition, Elsevier, Burlington, MA.
- Kwon, H. B., & Park, C. S. (2006). An Experimental Study on the Relationship between Ballast-Flying Phenomenon and Strong Wind under High-Speed-Train. *7th World Congress on Railway Research*. Montreal.
- Krylov, V. (1995). Generation of ground vibrations by superfast trains. *Journal of applied acoustics* (pp. 149-164).
- Krylov, V., Dawson, A. R., Heelis, M. E., Collop, A. C. (2000) Rail movement and ground waves caused by high-speed trains approaching track-soil critical velocities. *Journal of Rail and Rapid Transit*, 107-116.
- Landell, K. D., Lineker, R. L. (1962) Brake shoe key. *U.S. Patent No. 3,015,372*.
- Lazaro, B., Gonzalez, E., Rodriguez, M., Osma, S., Iglesias, J. (2011). Characterization and Modeling of Flying Ballast Phenomena in High Speed Lines. *9th World Congress on Railway Research*. Lille.

- Lazaro, B., Rodriguez-Plaza, M., Gonzalez, E., Mascaraque, A., Rodriguez, M. (2013) Test procedure for quantitative ballast projection risk evaluation. *International workshop on railway aerodynamics*. Birmingham, UK.
- Luo, Y., Yin, H., & Hua, C. (1996). The dynamic response of railway ballast to the action of trains moving at different speeds. *Journal of Rail and Rapid Transit*, 95-101.
- Macey, L. D. (2009). Electrical rail coupler assembly. *U.S. Patent No. 7,575,462 B2*.
- Madshus, C. & Kanya, M. (2000). High-speed railway lines on soft ground: dynamic behaviour at critical train speed. *Journal of Sound and Vibration*, 689-701.
- Portillo, I.A., Kaltenbach, H. J., Schober, M. (2008). The generic underfloor geometry laboratory experiment "BIAC". *Aerodynamics in Open Air* (pp. 21-26), Munich. DEUFRAKO.
- Quinn, A., & Hayward, M. (2008). Full scale aerodynamic measures underneath a high speed train. *BBA VI International Colloquium*, Milan.
- Quinn, A., Hayward, M., Baker, C. J., Schmid, F., Priest, J. A., & Powrie, W. (2010). A full-scale experimental and modelling study of ballast flight under high-speed trains. *Journal of Rail and Rapid Transit*, 61-74.
- Rocchi, D., Ripamonti, F., Viola, I., Gregoire, R., Guiloteau, E. (2008). Simulation on the ETR 500 train. *Aerodynamics in Open Air* (pp. 61-66). Munich: DEUFRAKO.
- Ruter, A. (2008). Full scale CFD investigation of the ICE 3 endcar (first bogie). *Aerodynamics in Open Air* (pp. 47-54). Munich: DEUFRAKO.
- Rüter, A., Schroeder-Bodenstein, K. (2008). Probabilistic assessment of the formation of ballast projection. *Aerodynamics in Open Air* (pp. 105-112). Munich: DEUFRAKO.
- Saussine, G., Paradot, N. (2008a). Full-scale tests on ballast track in wind tunnel. *Aerodynamics in Open Air* (pp. 93-98). Munich: DEUFRAKO.
- Saussine, G., Paradot, N. (2008b). Numerical analysis of the collision process between ballast grains and ballast bed. *Aerodynamics in Open Air* (pp. 89-92). Munich: DEUFRAKO.
- Saussine, G., Allain, E., Paradot, N., & Gaillot, V. (2011). Ballast flying risk method for high speed line. *9th World Congress on Railway research*. Lille.
- Saussine, G., Allain, E., Vaillant, A., Ribourg, M., & Neel, O. (2013). High speed in extreme conditions: ballast projection phenomenon. *International Workshop on Train Aerodynamics*. Birmingham.

- Schroeder-Bodenstein, K. (2008). Full-scale experiment on the ballast bed impact of particles. *Aerodynamics in Open Air* (pp. 83-88). Munich: DEUFRAKO.
- Sima, M. (2008). Full-scale CFD investigation of the ICE 3 train set (midcar). *Aerodynamics in Open Air* (pp. 55-60). Munich: DEUFRAKO.
- Sima, M. (2008). Mesh design for the generic underfloor geometry and for the ICE-3. *Aerodynamics in Open Air* (pp. 35-40). Munich: DEUFRAKO.
- United States White House (2014). <http://www.whitehouse.gov/blog/09/04/16/A-Vision-for-High-Speed-Rail/>. Accessed 20 January 2014.
- Van Vulpen, J. (1939). Flexible metallic hose. *U.S. Patent No. 2,150,471*.
- Weise, M. (2012). *TSI and CEN norm text proposal for evaluation method and limit for aerodynamic loads on track*. Bombardier Transportation GmbH. AeroTRAIN.

Abbreviations and Acronyms

ADIF	Administración de Infraestructuras Ferroviarias de España
BFPF	Ballast Flight Probability Factor
BIAC	Bogies in a Channel
CFD	Computational Fluid Dynamics
DB	Deutsche Bahn
DES	Detached Eddy Simulation
DOT	Department of Transportation
EIS	Environmental Impact Statement
FE	Finite Element
FEC	Florida East Coast Railway
FRA	Federal Railroad Administration
FS	Ferrovie dello Stato Italiane (Italian State Railways)
HSL	High-Speed Line
HSR	High-Speed Rail
LES	Large Eddy Simulation
PDF	Probability Density Function
NEC	North East Corridor
NS	Navier-Stokes equations
PoliMI	Politecnico di Milano
RailTEC	Rail Transportation and Engineering Center
RANS	Reynolds Averaged Navier-Stokes
RFI	Rete Ferroviaria Italiana
ROD	Record of Decision
ROW	Right-of-Way
SNCF	Société Nationale des Chemins de fer Français
UPM	Universidad Politécnica de Madrid